The CRDS spectrum of acetylene near 1.73 μm

Oleg Lyulin, Semen Vasilchenko, Didier Mondelain, Alain Campargue

The CRDS spectrum of acetylene near 1.73 µm

Oleg Lyulin[1,2], Semen Vasilchenko[1,2], Didier Mondelain[1], Alain Campargue[1*]

[1] Univ. Grenoble Alpes, CNRS, LIPhy, *38000 Grenoble, France*

[2] V.E. Zuev Institute of Atmospheric Optics SB RAS,*1, Academician Zuev square, Tomsk 634021, Russia*

Number of Pages: 25
Number of Figures: 8
Number of Tables: 2

Running Head: *Acetylene near 1.74 µm*

Keywords: *acetylene; C_2H_2; line intensity; CRDS; spectroscopic database; HITRAN*

* Corresponding author
Tel: +33 4 76 51 43 19
E-mail address: Alain.Campargue@univ-grenoble-alpes.fr

Friday, January 10, 2020

ABSTRACT

The high-resolution absorption spectrum of acetylene has been recorded at room temperature by high sensitivity cavity ring down spectroscopy (CRDS) in the 5693-5882 cm^{-1} region. The noise level of the recordings corresponds to a typical minimum detectable absorption, α_{min}, below 10^{-10} cm^{-1}. The positions and intensities of about 4000 lines were determined and analyzed together with about 3900 lines left unassigned in a previous CRDS study in the 5850-6340 cm^{-1} region (*OM Lyulin, D. Mondelain, S. Béguier, S. Kassi, J. Vander Auwera, A. Campargue. High sensitivity absorption spectroscopy of acetylene by CRDS between 5851 and 6341 cm^{-1}. Mol Phys,* ***112****, 2433–44 (2014)).* In total, about 2620 $^{12}C_2H_2$ and 250 $^{12}C^{13}CH_2$ absorption lines are assigned in the present work, most of them being newly reported. The $^{12}C_2H_2$ lines belong to 53 bands and include 24 bands newly identified or improved in the region of the previous study. Altogether, 107 bands in the entire 5693-6340 cm^{-1} while the HITRAN database provides line parameters of only nine $^{12}C_2H_2$ bands in the same region. The lines of $^{12}C^{13}CH_2$ in normal abundance (2.2 %) belong to eight bands whose intensities are reported for the first time. Spectroscopic parameters of the upper vibrational levels were derived from standard band-by-band fits of the line positions (typical *rms* values of the (obs.-calc.) deviations are better than 0.002 cm^{-1}). The vibrational transition dipole moment squared and Herman-Wallis coefficients of each band were derived from a fit of the measured intensity values. A recommended line list is provided for the bands newly assigned with positions calculated using empirical spectroscopic parameters of the lower and upper energy vibrational levels and intensities computed using the derived Herman-Wallis coefficients. As a result, the constructed line list includes a total of 4471 transitions belonging to 53 bands of $^{12}C_2H_2$ and 8 bands of $^{12}C^{13}CH_2$. This list of acetylene transitions above 5693 cm^{-1} extends to lower energy and completes our empirical spectroscopic database for acetylene in the 5850-9415 cm^{-1} range.

1. Introduction

Up to the visible spectral region, the acetylene absorption spectrum is organized into polyads of vibrational states in strong resonance interaction [1-6 and reference therein]. Each polyad is characterized by a polyad quantum number, $P= 5V_1+3V_2+5V_3+V_4+V_5$, where V_i are the conventional vibrational normal modes quantum numbers, and i= 1-5 correspond to the symmetric CH and CC stretching modes, the antisymmetric CH stretch, and the *trans*- and *cis*-degenerate bending modes, respectively. The latter being characterized by the bending angular momentum quantum numbers, l_4 and l_5. The present contribution takes part in a long term project aiming at constructing an empirical database for acetylene in the near infrared. Indeed, in spite of being the most studied four-atoms molecule and of increasing needs for planetary applications, the status of the spectroscopic databases of acetylene (C_2H_2) in the near infrared is far to be satisfactory both in terms of completeness and accuracy. For instance, in its last version, the HITRAN database [7] provides only the few strongest bands for each ΔP variation of the polyad quantum number. While a number of studies have been devoted to rovibrational assignments and line positions analysis [4-6,8-10], intensity information is generally missing which prevents the inclusion of these data in spectroscopic databases. This is for instance the case of the extensive study reported by Keppler et al. [9] by Fourier-transform spectroscopy (FTS) with a 352.5 m pathlength in the 1.4-1.7 µm region which partly overlapped our region of interest. In addition, due to the number and strength of rovibrational interactions, the rovibrational assignment of high sensitivity spectra of acetylene is a challenge in the near infrared because many hot bands including perturbed bands are overlapping leading a highly congested spectrum with no apparent regular structure, except for the few strongest bands.

In 2017, we constructed a spectroscopic database for acetylene in the wide 5850-9415 cm^{-1} region (excluding the 6341-7000 cm^{-1} interval) [11] by gathering results of six studies by Fourier-transform spectroscopy (FTS) in the region of the strong bands [12-14] and cavity ring down spectroscopy (CRDS) in the region of weak absorption intervals between the bands [15-17]. Compared to the HITRAN [7] and GEISA [18] spectroscopic databases in the region, the number of bands and lines (179 and 11113, respectively) was increased by more than a factor of ten. In our database, the acetylene line positions are calculated using empirical spectroscopic parameters of the lower and upper energy vibrational levels and intensities are computed using the vibrational transition dipole moment squared and Herman-Wallis coefficients derived, for each band, from a fit of measured intensities. This approach allowed completing the experimental list by adding missing lines and improving poorly determined positions and intensities. Note that, very recently we extended the database towards higher energy from the analysis of an FTS spectrum in the 9280-10740 cm^{-1} interval [19,20].

In the present study, the CRDS spectrum in the 5693-5882 cm^{-1} region is considered. This study extends to lower energy a previous CRDS investigation in the 5851-6341 cm^{-1} [16] where about 4600 absorption features were left unassigned. The assignment of the spectrum is performed by

comparison to the predictions of a global effective model developed at IAO-Tomsk for $^{12}C_2H_2$ [21] This global model is the basis of the recently released Acetylene Spectroscopic Databank (ASD) [22]. The ASD line positions are calculated on the basis of a global effective Hamiltonian (EH) with parameters values fitted against an exhaustive review of the $^{12}C_2H_2$ line positions available in the literature. Line intensities are calculated using the corresponding EH eigenfunctions and an effective dipole moment (EDM) with parameters fitted against experimental intensities, for each ΔP value. The assignment of the CRDS spectra of Ref. [16] relied on a previous version of the model predictions which were updated in the recent ASD on the basis off enlarged datasets including the positions and intensities reported in Ref. [16]. As a result, the predictive capabilities of the model in the region are improved. This is the reason why, in the present work, together with the analysis of newly recorded region, we reconsider the unassigned lines of Ref. [16] in the 5850-6340 cm^{-1} region.

2. Experimental details and line list construction

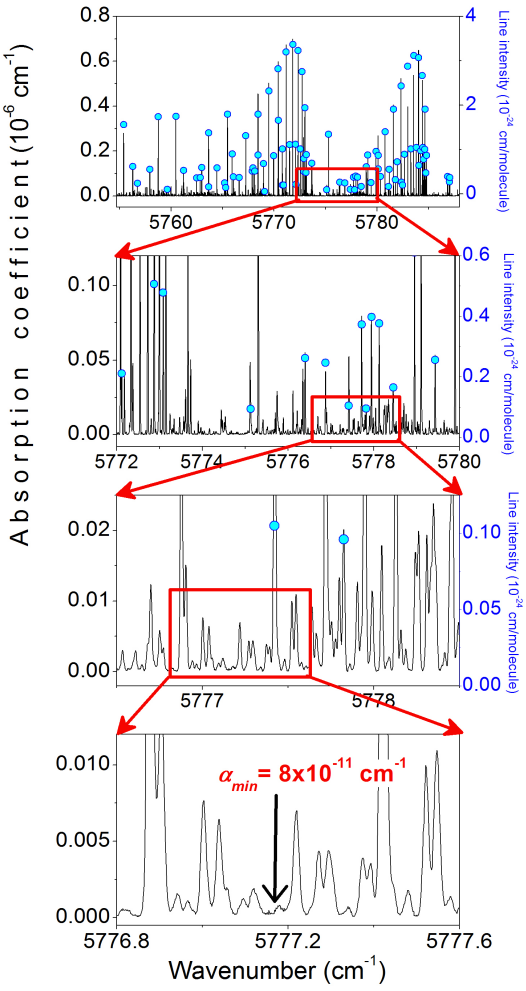

Fig. 1
CRDS spectrum of acetylene near 5770 cm^{-1} illustrating the richness of the spectrum and the spectral congestion. The sample pressure was 0.10 Torr. Four successive enlargements illustrate the high dynamics of the recordings giving access to absorption coefficients from 10^{-6} cm^{-1} to the noise level α_{min}~ 8×10^{-11} cm^{-1}. The comparison to the HITRAN line list (blue dots) displayed on the three upper panels shows that the large amount of acetylene lines newly measured.

The reader is referred to Ref. [23] for a general description of the CRDS setups developed in our group. Fibered distributed feed-back (DFB) laser diodes are used as light source. Using a set of eight DFB laser diodes (from Eblana Photonics), the 5695-5900 cm^{-1} spectral interval has recently become accessible to our CRDS spectrometer. The setup was already used for a high sensitivity characterization of the spectra of water isotopically enriched in ^{17}O [24], N_2O [25] and carbon dioxide in its 1.75 µm transparency window [26,27]. Each laser diode tuning ranges about 20 cm^{-1} by temperature tuning from -5°C to 55°C allowing for the coverage of the 5692.95-5882.17 cm^{-1} range with only a few spectral gaps: 5715.8-5723.0, 5744.5-5747.9, 5809.0-5810.2 and 5851.7-5855.8 cm^{-1}.

The finesse of the cavity varied from 130,000 at 5850 cm^{-1} to 200,000 at 5700 cm^{-1} resulting in measured ring down (RD) times from 200 µs to 300 µs, respectively. About 30 to 100 RD events were averaged per spectral point.

An acetylene sample free of acetone and in normal isotopic abundance was used to fill the cell at a pressure of 0.10 Torr. The cell temperature was measured with a temperature sensor (TSic 501, IST-AG, 0.1 K accuracy) fixed on the cell surface, covered by an external blanket of foam for thermal isolation. During the recordings reported here, the cell temperature varied between 293.4 and 295.1 K. The gas pressure was continuously measured by a capacitance gauge (MKS Baratron, 10 Torr, 0.25 % accuracy of the reading).

During the spectrum recording, a wavemeter measured the wavenumber of the laser emission at each spectral step of typically 0.002 cm^{-1} giving a first frequency calibration of the spectrum. This calibration was then refined using accurate C_2H_2 line positions provided by the HITRAN2016 database [7]. This leads to an estimated uncertainty of 1×10^{-3} cm^{-1} on the line center determination of unblended lines.

The minimum detectable absorption coefficient (evaluated as the *rms* of the base line fluctuation), α_{min}, varies between 1×10^{-10} cm^{-1} and 6×10^{-11} cm^{-1} depending on the RD time. As a result, line intensities spanning more than three orders of magnitude (from 5×10^{-24} to 10^{-27} cm/molecule) could be retrieved from the measured spectra. The successive enlargements of the spectra presented in **Fig. 1** illustrate the sensitivity and high dynamic range of the recordings and the noise level on the order of $\alpha_{min}\sim 8\times10^{-11}$ cm^{-1}. In the investigated region, the acetylene spectrum is not particularly weak (strongest lines have intensity on the order of 10^{-23} cm/molecule). This is the reason why a pressure value of 0.1 Torr was sufficient to detect many new lines. In **Fig. 1,** the HITRAN line list superimposed to the recorded spectrum shows the large amount of newly detected transitions. The high spectral congestion (about 20 lines/cm^{-1}) made the rovibrational assignment particularly laborious.

A homemade multiline fitting computer code was used to derive the line positions and intensities. The line shape was modeled with the Voigt profile with Gaussian width calculated for $^{12}C_2H_2$ Doppler broadening. The Doppler half width at half maximum of the line shape (HWHM) is about 0.007 cm^{-1} while the average pressure self-broadening of 0.14 cm^{-1}/atm [7] leads to a negligible

Lorentzian contribution of about 2×10^{-5} cm^{-1}. The spectrum is very dense so the accuracy of the reported intensities depends on the weakness and overlapping of the considered lines. In the case of relatively strong isolated lines, we estimate to 5% the uncertainty on the line intensity. Overall, line centres and intensities were derived for a set of about 4000 lines. Using HITRAN2016 database a number of water lines was removed from the line list, leaving about 3800 lines to be assigned in the 5693-5882 cm^{-1} region.

3. Rovibrational assignments

An overview of the line lists at disposal is presented in **Fig. 2**. The 5693-6341 cm^{-1} displayed interval includes the region above 5851 cm^{-1} investigated in Ref. [16]. On the upper panel, the list of transitions above 5850 cm^{-1} as assigned in Ref. [16] is displayed together with the HITRAN line list. The middle panel shows the list of lines at disposal for new assignments. It consists in the list of lines retrieved from the new spectra in the 5693-5882 cm^{-1} region (about 4100 lines) complemented by about 3900 unassigned lines of Ref. [16], above 5882 cm^{-1} and in the 5851.7-5855.8 cm^{-1} interval which corresponds to a gap of the present recordings for which no new spectra were recorded The lower panel shows the list of lines assigned in the present study, thus a subset of the data presented in the middle panel.

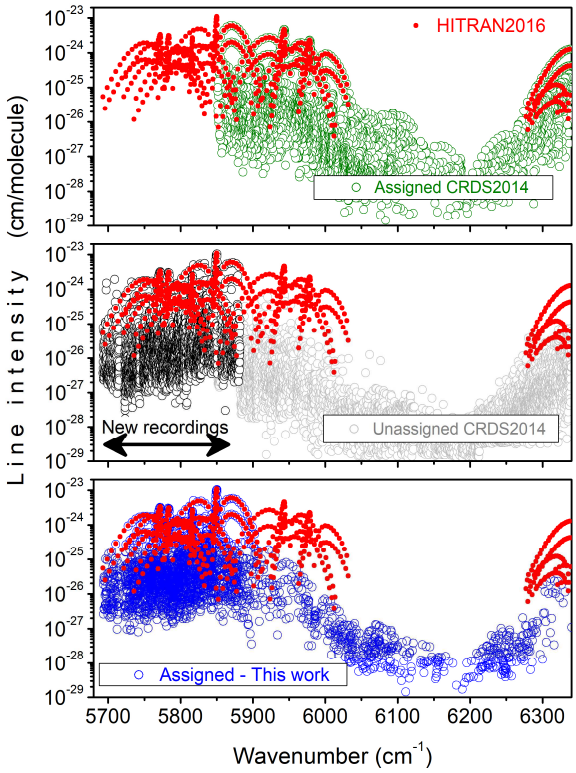

Fig. 2.
Different line lists for acetylene in the 5695-6340 cm^{-1} region.
Upper panel: Acetylene transitions assigned in Ref. [16] above 5851 cm^{-1} (green open circles) and HITRAN2016 database (red dots),
Middle panel: Line list under analysis consisting of the list retrieved from new CRDS recordings below 5882 cm^{-1} (black open circles) and lines left unassigned in the analysis of Ref. [16] (grey open circles),
Lower panel: Subset of the middle panel limited to the lines assigned in this work (blue open circles).

As mentioned above, the $^{12}C_2H_2$ rovibrational assignment was performed on the basis of the predictions of the Tomsk effective Hamiltonian model developed in the frame of the effective operator approach [21]. This model considers all the resonance interactions between rovibrational levels up to the ninth order of perturbation theory. Effective rovibrational parameters were adjusted to reproduce more 30000 measured line positions collected from the literature up to 9900 cm^{-1}, including those from Ref. [16]. All but five bands reported in this work correspond to *a* ΔP= 9 variation of the polyad quantum number. The five remaining bands, located above 6250 cm^{-1}, correspond to ΔP= 10. The calculation of the line intensities requires a set of effective dipole moment (EDM) parameters for each ΔP value. The ΔP= 9 EDM parameters used in the construction of the line list of Ref. [22] relied on a few FTS measurements of the strongest bands [28] and on the large set of intensity values reported in Ref. [16]. The presence of a *Q* branch, the observation of the 1:3 intensity alternation from even to odd values of *J* and lower state combination difference (GSCD) relations were systematically used as additional criteria to confirm the assignments.

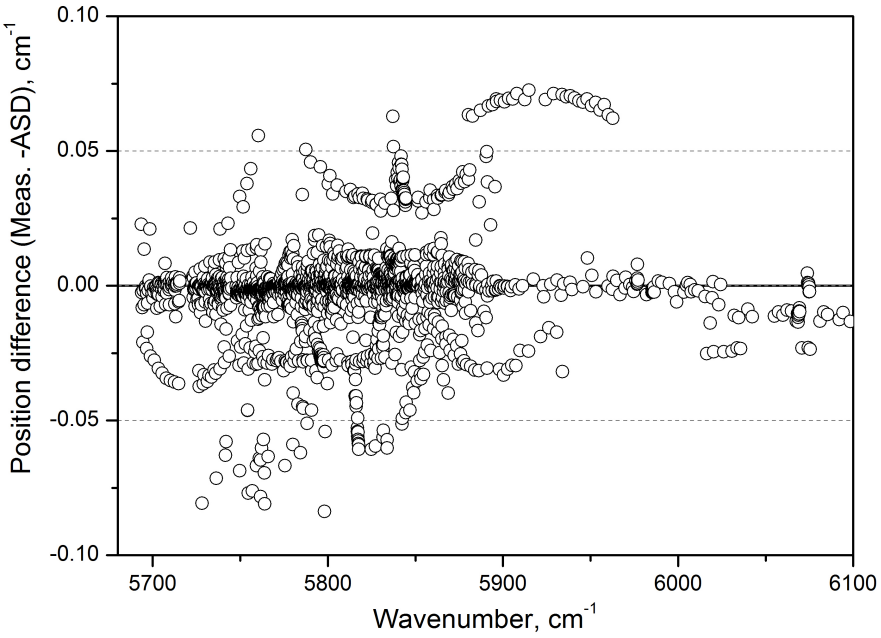

Fig. 3.
Comparison of the measured positions of $^{12}C_2H_2$ with corresponding calculated values included in the Acetylene Spectroscopic Databank [22] in the 56980-6100 cm^{-1} region.

Overall, 2627 lines were assigned to fifty-three $^{12}C_2H_2$ bands, most of them being newly reported and located in the newly recorded region. The deviations between measured and ASD predicted line positions are plotted on **Fig. 3** *versus* the wavenumber. As expected, the largest deviations (up to 0.1 cm^{-1}) correspond to lines located in the newly recorded region, as the ASD list took into account the CRDS data of Ref. [16] above 5850 cm^{-1}.

The assigned bands are listed in **Table 1** in increasing order of the upper state energy. In the first column, we provide the ($v_1v_2v_3v_4v_5l_4l_5\varepsilon$) normal mode labeling and symmetry type *(e* or *f)* relative to the Wang transformation. The vibrational labeling is obtained from the global effective Hamiltonian [21] and usually corresponds to the maximum fraction of the low *J* eigenfunctions in the normal mode basis. In order to avoid duplicate vibrational labeling, we chose one of the major contributors for the labeling of the states at 5893.26 and at 7787.32 cm^{-1}. We also give the band name in the vibrational notation of Plíva adopted in the HITRAN database: $\nu_1\nu_2\nu_3(\nu_4\nu_5)^{\ell\pm}r$ with $l=|l_4+l_5|$, l_t being the vibrational angular momentum quantum number associated with the degenerated bending mode *t*, ± being the symmetry type for Σ vibrational states (l= 0), and *r* a roman numeral indicating the rank of the level, by decreasing energy value (r= *I* for the highest energy level), inside the set of states having the same *l* value.

The assignment of the four vibrational bands provided by the HITRAN database in the 5693-5882 cm^{-1} region (see **Table 1**) was extended towards higher *J* rotational quantum number. In the 5850-6340 cm^{-1} region reported in Ref. [16], fifteen bands were identified among the set of unassigned lines and the analysis of nine bands was improved. For example, the *P* branches of the $\nu_2+\nu_3+(\nu_4+\nu_5)^0-\nu_5^1$ and $\nu_2+\nu_3+(\nu_4+\nu_5)^2-\nu_5^1$ hot bands at 5836.12 and 5844.64 cm^{-1}, located in the newly recorded region, could be assigned. The assignment of the $\nu_1+(3\nu_4+\nu_5)^{0+}$ at 5865.56 cm^{-1} band was greatly extended, mainly in the *P* branch. The number of observed transitions in the $\nu_2+\nu_3+2\nu_4^2-\nu_4^1$ band at 5836.11 cm^{-1} was increased from 19 to 103. The assignment of the transitions reaching *f* upper level of the $2\nu_2+(\nu_4+3\nu_5)^0-\nu_4^1$ hot band given in Refs. [11,16] was corrected. Overall, forty bands are reported for the first time. Part of the upper vibrational states were already observed as upper levels of different bands located in other spectral regions but thirteen upper states, marked "N" in **Table 1**, are new. Additionally, transitions to *f* sublevels of the $v_1v_2v_3v_4v_5l_4l_5$= 02013-13, 0201311 and 1013030 vibrational states are observed for the first time from the $2\nu_2+(\nu_4+3\nu_5)^2$II-ν_4^1, $2\nu_2+(\nu_4+3\nu_5)^2$I-ν_4^1 and $\nu_1+\nu_3+3\nu_4^3-(\nu_4+2\nu_5)^3$ bands, respectively, while transitions to their *e* sublevels were already reported in the literature from the bands $2\nu_2+(\nu_4+3\nu_5)^2$II, $2\nu_2+(\nu_4+3\nu_5)^2$I [29] and $\nu_1+\nu_3+3\nu_4^3-2\nu_4^2$ [12]. The assigned bands include three "forbidden" bands with ΔK= 2 and four with ΔK= 3. (K= *l* for linear molecules). As an illustration of the sensitivity of the CRDS recordings, let us mention *(i)* the unexpected detection of the $2\nu_2+(3\nu_4+\nu_5)^4-\nu_4^1$ band reaching the "exotic" 0203131 upper state with K= 4 and *(ii)* the detection of the $3\nu_3-\nu_1$ hot band near 6267.02 cm^{-1} from the v_1= 1 lower state at 3372.85 cm^{-1} with a relative population of only about 8×10^{-8}.

Finally, 248 transitions of eight bands of $H^{12}C^{13}CH$ in natural abundance in our sample (2.2 %) were identified. Their identification relied on the extensive study by Di Lonardo performed by FTS with 99% enrichment in $H^{12}C^{13}CH$ and a 55.1 m pathlength [30] (the corresponding line positions can be found in Ref. [31]). No intensity information was reported in Refs. [30,31]. Although of limited

accuracy due to their weakness and frequent overlapping in our CRDS acetylene spectrum, the intensity of the $H^{12}C^{13}CH$ bands are, to the best of our knowledge, the first ones reported in the region.

4. Band by band analysis.

4.1. Spectroscopic parameters

The rotational analysis was performed using the standard formula for the rovibrational energy levels of an isolated vibrational state:

$$T(v, J, e/f) = G_{e/f} + B_{e/f}J(J+1) - D_{e/f}[J(J+1)]^2 + H_{e/f}[J(J+1)]^3 \qquad (1)$$

Where $G_{e/f}$ is the vibrational term value and $B_{e/f}$, $D_{e/f}$, and $H_{e/f}$ are the rotational and distorsion constants of the *e* and *f* sub levels. The parameters of the lower vibrational levels were constrained to their fitted values of Refs. [16,32], except for the 0001212 and 1000000 levels. The spectroscopic constants of these two levels, included in **Table 1**, were determined from a fit of the line positions of the $(\nu_4+2\nu_5)^3$-$(2\nu_4+\nu_5)^3$ and ν_1 - ν_5^1 bands reported in Refs. [33,34]. As the *e* and *f* sub bands may be perturbed in a different way, different sets of spectroscopic parameters were fitted for the *e* and *f* levels. When a given sublevel was observed through transitions from different lower levels, its spectroscopic parameters were obtained from a simultaneous fit of the line positions of the different sub-bands. The retrieved constants of the lower and upper states are listed in **Table 1**. The results of the fit are provided for each band in the Supplementary Material I. The bands of Ref. [16] which were updated or extended in the present work are indicated by "Luy14".

Some of the studied bands were found to be affected by perturbations (they are marked with "P" in **Table 1**). In the cases where the perturbation does not allow reproducing the rotational structure using Eq. (1), the levels with high rotational quantum number were excluded from the fit. After exclusion of the lines with poorly determined centers or affected by perturbation, the average *rms* values of the (meas.-fit) differences are on the order of 1.5×10^{-3} cm^{-1} which is close to our claimed accuracy on the measured line positions. The distortion constants of the perturbed bands are usually anomalously large or negative. Two examples of the results of the fit of perturbed bands leading to effective parameters values are presented in **Fig. 4**.

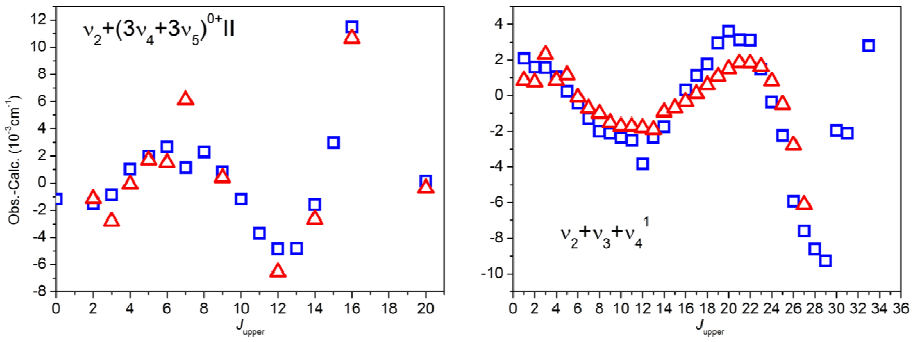

Fig. 4.
Examples of perturbed bands. The data represent the differences between the measured line positions and their values calculated using retrieved spectroscopic constants. The blue squares and red triangles correspond to the *P* branch and *R* branch, respectively.

5. Line intensities.

Let us consider an absorption line corresponding to the $V'J'\varepsilon' \leftarrow VJ\varepsilon$ transition in a linear molecule (V and J are the vibrational index and the angular momentum quantum number, respectively, and ε= ± is the parity). The intensity of the considered transition, $S_{V'J'\varepsilon'\leftarrow VJ\varepsilon}$ (in cm/molecule), at a temperature T (in K) is related to the transition dipole moment squared $|R|^2$:

$$S_{V'J'\varepsilon'\leftarrow VJ\varepsilon}(T) = \frac{8\pi^3}{3hc} C g_{VJ\varepsilon} \frac{\nu_{V'J'\varepsilon'\leftarrow VJ\varepsilon}}{Q(T)} \exp\left(-\frac{hcE_{VJ\varepsilon}}{kT}\right)\left[1-\exp\left(-\frac{hc\nu_{V'J'\varepsilon'\leftarrow VJ\varepsilon}}{kT}\right)\right] L(J,K)\left|R\right|^2 \quad (2)$$

where $E_{VJ\varepsilon}$ is the lower state energy and $\nu_{V'J'\varepsilon'\leftarrow VJ\varepsilon}$ is the transition wavenumber, $Q(T)$ is the total internal partition function at temperature T, C is the isotopic abundance, and $g_{VJ\varepsilon}$ is the nuclear statistical weight of the lower state and *L(J,K)* is Hönl-London factor. The values of the total internal partition function of $^{12}C_2H_2$ and $^{12}C^{13}CH_2$ were deduced from the data tabulated in Ref. [35]. The $^{12}C_2H_2$ and $^{12}C^{13}CH_2$ natural isotopic abundances were fixed to their HITRAN values (0.9776 and 0.02197, respectively).

The expression of the Hönl-London factors for parallel (ΔK= 0), perpendicular (ΔK = ±1) and ΔK = ±2 forbidden bands can be found in Ref. [11], and in Ref. [36] for ΔK = ±3. To reduce the data, effective parameters can be deduced expanding $|R|^2$ empirically to take account for the rotational dependence:

$$|R|^2 = |R_0|^2 (1 + A_1^{RP} m + A_2^{RP} m^2)^2 \text{ (}P\text{- and }R\text{-branches)}, \quad (3)$$

$$|R|^2 = |R_0|^2 (1 + A_2^{Q} m^2)^2 \text{ (}Q\text{-branch)}, \quad (4)$$

m being equal to $-J$ in the P-branch, J+1 in the R-branch, and J in the Q-branch. $|R_0|^2$ is the vibrational transition dipole moment squared, and A_1^{RP}, A_2^{RP}, and A_2^{Q} are the Herman-Wallis coefficients. Note that we use the squared form of the terms between parentheses in Eqs. (3,4) accordingly to our previous publication [11].

Vibrational transition dipole moments squared and Herman-Wallis coefficients obtained from an unweighted fit of the experimental intensity values are reported in **Table 2**. The calculated line intensities and the relative differences from their measured values are included in Supplementary Material I, for every band. As a result of the frequent line overlapping and of the weakness of many bands, a significant number of line intensities are not sufficiently accurate and were excluded from the fit. The transitions ignored in the intensity fit are marked with "i" in the Supplementary Material. Very often, different sublevels of a given band could not be fitted with the same set of empirical parameters. Assuming that it is due to different perturbation mechanisms, we provide in these cases different sets of empirical parameters for each-sub band. The root mean square deviation of the intensity fit given by the fitting procedure is included in **Table 2**. In many cases, in view of the number of intensity values which were excluded, it seems that the obtained *rms* values overestimate the quality of the fits and we give in the last column of **Table 2** our own estimation of the relative error bars of the intensities

calculated with the obtained set of parameters. Some weak bands show a very irregular rotational intensity distribution. Although poorly reproduced by the fit, these bands are kept in **Table 2** (with a 50 %) error bar) because the knowledge of the order of magnitude of the band strength is a valuable information.

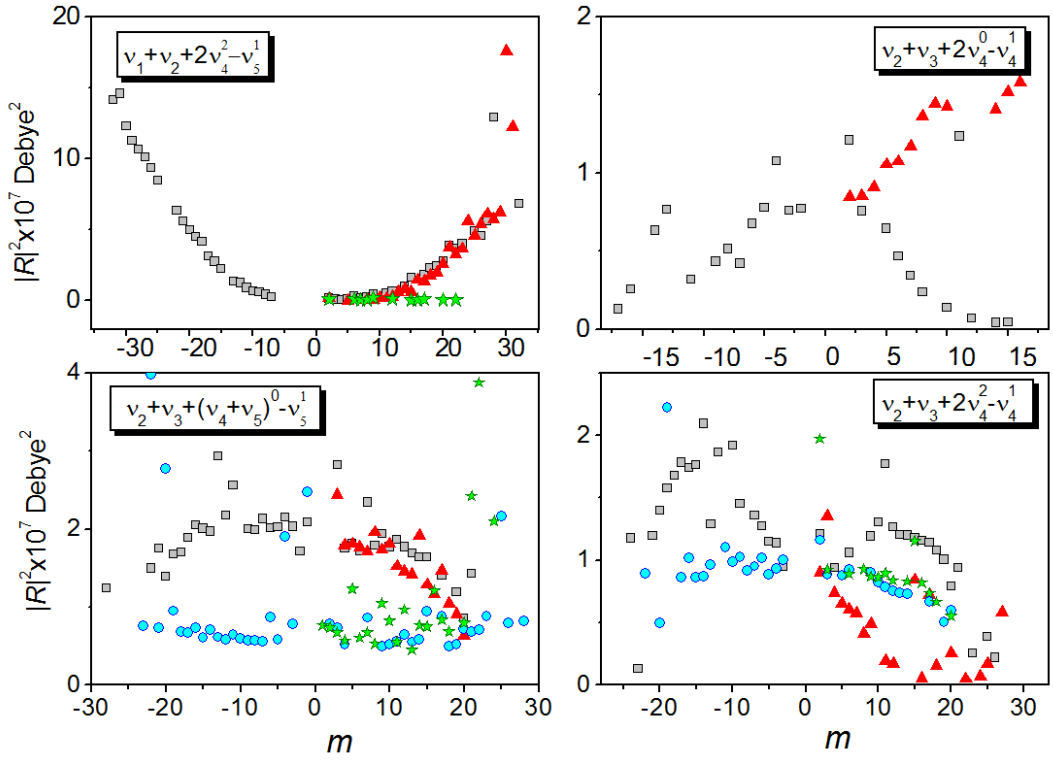

Fig. 5.
Four examples of the line intensity fits of the different sub-bands of hot bands (see details in the text). Black squares and blue circles correspond to $|R|^2$ values of the *e-e* and *f-f* transitions, respectively, while red triangles and green stars correspond to the *e-f* and *f-e* transitions in the *Q* branche. (*m* stands for $-J$, J, $J+1$ for *P, Q, R* branches, respectively).

In **Fig. 5** are presented four interesting examples of the rotational dependence of the transition dipole moment squared. One can see that different parameters had to be used for describing the rotational dependence of the different *Q*-branches of the $\nu_1+\nu_2+2\nu_4^2-\nu_5^1$ band. The $\nu_2+\nu_3+2\nu_4^0-\nu_4^1$ hot band shows an unusual rotational dependence of the transition dipole moment squared in the *R* branch. The vibrational transition dipole moments squared of the different sub bands of the $\nu_2+\nu_3+(\nu_4+\nu_5)^0-\nu_5^1$ band are very different. Finally, the *e-e*, *f-f*, *e-f* and *f-e* sub bands of the $\nu_2+\nu_3+2\nu_4^2-\nu_4^1$ band have different set of parameters.

6. Recommended empirical line list

On the basis of the empirical parameters obtained, a recommended acetylene line list was generated for each band listed in **Table 2** for the reference temperature of 296 K, following the same method as adopted in Ref. [11]. For each branch of a given band, the line list was calculated for all the transitions up to a maximum J value exceeding by 1 the largest J value of the observations. Line positions were computed using the spectroscopic constants of **Table 1** and line intensities were

obtained from $|R_0|^2$ and Herman-Wallis factors collected in **Table 2**. This approach allows completing the experimental observations by interpolation between measured lines and slightly extends beyond the observations. This is especially important in the case of weak bands, where a significant number of lines are obscured by strong ones. These advantages are illustrated in **Fig. 6** by the example the $\nu_2+(3\nu_4+3\nu_5)^{0+}$I band at 5921.92 cm^{-1}.

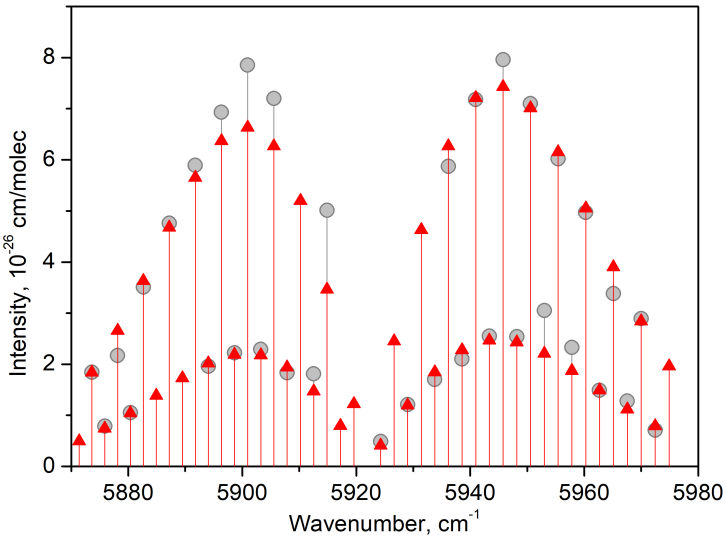

Fig. 6.
Comparison of the measurements (circles) to the obtained recommended empirical line list (triangles) for the band $\nu_2+(3\nu_4+3\nu_5)^{0+}$I at 5921.92 cm^{-1}.

As discussed in Ref. [11], a number of bands are perturbed and cannot be reproduced using an isolated band model. Additionally, there are cases of local perturbation around some *J* value due to a crossing with energy levels of a perturber state. In such cases, and also in the cases where calculated intensity values were anomalously large we kept in the recommended line list the measured intensity values, marked them with an "e" label. Moreover, we did not perform any interpolation or extrapolation around such lines and, consequently, some *J* values may be missing in the rotational structure. The set of recommended line lists is provided as Supplementary Material 2. The recommended line list contains 3975 lines of $^{12}C_2H_2$ and 496 lines of $^{13}C^{12}CH_2$. The number of lines is given for every band in fifth column of **Table 2**. Note that the line list recommended in this work contains some bands already included in the recommended line list of Ref. [11] above 5850 cm^{-1}. These bands are noted in **Table 1** and should be removed from the list of Ref. [11] when the two recommended lists are merged. The direct comparison of the CRDS spectrum to the recommended lists displayed in **Fig. 7** shows that the lines left unassigned are generally weak (see also lower panel of **Fig. 2**).

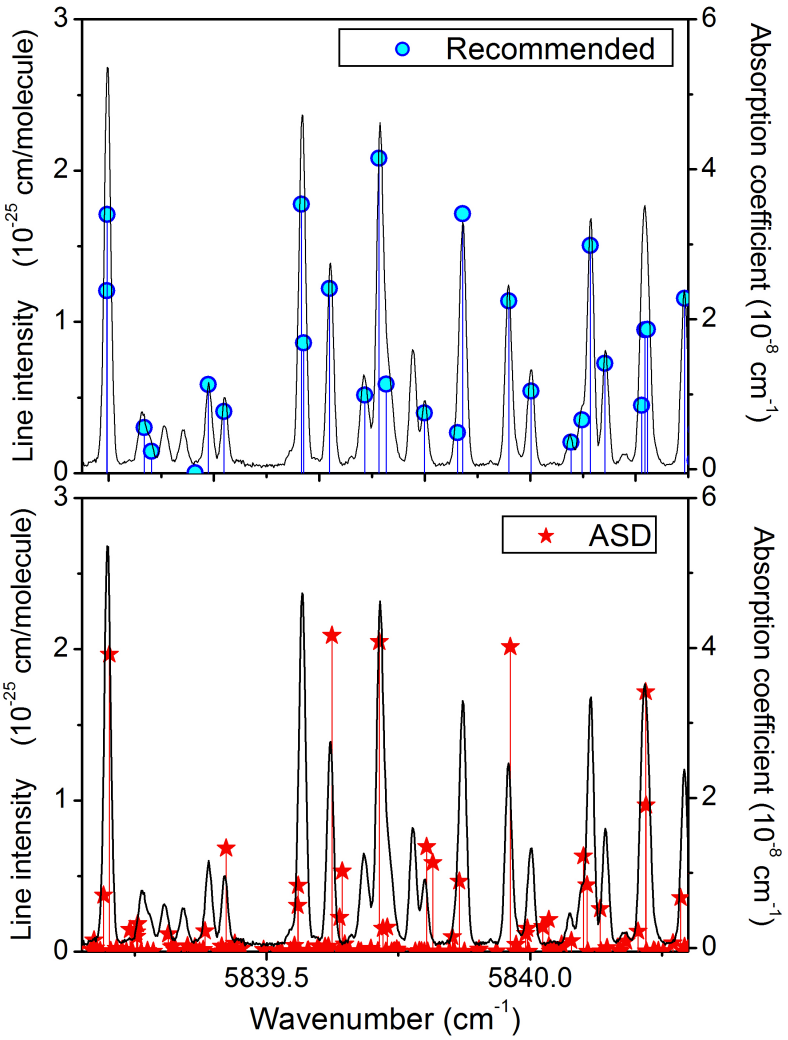

Fig. 7.
Comparison of the CRDS spectrum of acteylene to the recommended list obtained in this work (upper panel) and to acetylene sepctroscopic databank (ASD) of Ref. [22]. (lower panel).

5. Discussion and concluding remarks

In the region of the newly recorded spectra below 5882 cm^{-1}, the HITRAN2016 line list [7] provides spectroscopic information only for the four strongest bands: two Π_u–Σ_g^+ cold bands $(2\nu_2+(2\nu_4+\nu_5)^1\Pi$ and $\nu_2+\nu_3+\nu_4^1$ at 5816.86 and 5850.65 cm^{-1}, respectively) and two Σ_g^+–Π_u hot bands $(2\nu_3-\nu_5^1$, $\nu_1+\nu_2+2\nu_4^0-\nu_5^1$ at 5773.18 and 5784.84 cm^{-1}, respectively). Their line positions were calculated values in [37], using a polynomial expansion (Eq. (1)) with spectroscopic constants fitted against FTS position values from Refs. [9,28]. Line intensities provided by the HITRAN database were calculated in [37] using $|R_0|^2$ and Herman-Wallis coefficients derived from a fit of the FTS line intensities reported in Ref. [28]. The comparison of the HITRAN positions and intensities to those of our recommended line list is presented in **Fig. 8**. The intensity ratios show for each branch a break of the slope for a high J value. These breaks correspond to the highest J value of the measured intensities used in Ref. [37]. Jacquemart et al. extrapolated the intensities beyond J_{max} by fixing $|R|^2$ to the value corresponding to J_{max} which led to the observed breaks of slopes. Excluding HITRAN extrapolated

values, a systematic deviation on the order of 5-8 % is noted between our intensity values and those provided by the HITRAN database.

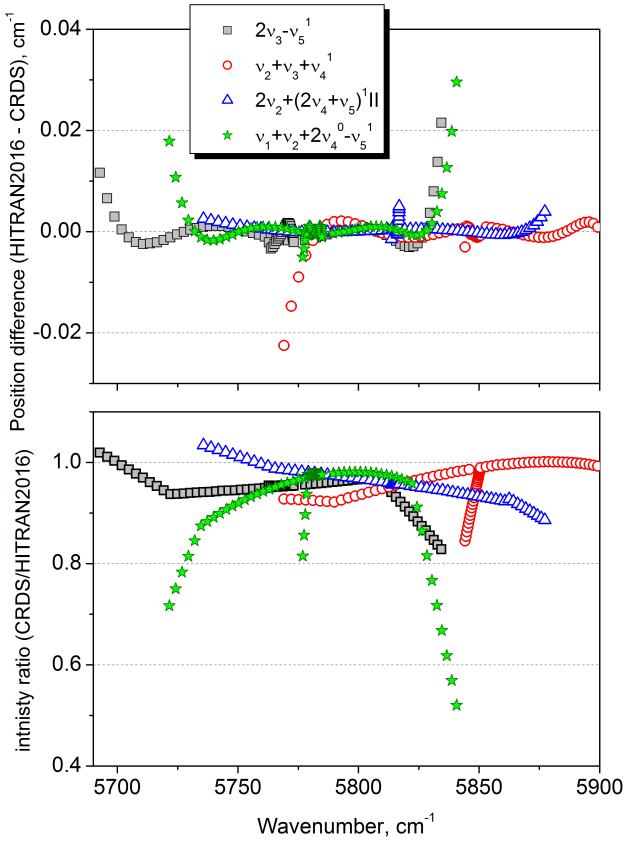

Fig. 8.
Comparison of the positions and intensities of the lines provided by the HITRAN2016 database for $^{12}C_2H_2$ to those recommended in pour list. The break of slopes observed for the intensity ratios is due to the HITRAN values (see Text).

As line positions are concerned, large deviations (more than 0.01 cm^{-1}) are observed in the range of HITRAN high *J* extrapolations. Our spectroscopic constants rely on a set of line positions significantly more extended than the FTS dataset used in Ref. [37]. As an example, in the case of the $\nu_1+\nu_2+2\nu_4^0-\nu_5^1$ band at 5784.84 cm^{-1}, the highest rotational line positions considered in Ref. [37] correspond to *P*(20), *Q*(21) and *R*(16) while the sensitivity of our recordings allowed for the measurement of the transitions up to *P*(32), *Q*(29) and *R*(28). The range of the HITRAN extrapolations beyond the FTS measurements is relatively large (up to *P*(25), *Q*(25) and *R*(15) in the above example) and thus somewhat hazardous. The uncertainty attached to the HITRAN positions has been increased from 0.001 to 0.01 cm^{-1} in the case of the extrapolated values. Some deviations exceeding this error bar are nevertheless observed.

In summary, the high-resolution CRDS absorption spectrum of acetylene has been recorded with unprecedented sensitivity and analyzed in the 5693-5882 cm^{-1} region. The predictions of the global model developed at IAO-Tomsk [21,22] have allowed assigning many new bands and extend assignment already known bands in this region and in the region 5850-6340 cm^{-1} analyzed several

years ago. Overall, 2627 $^{12}C_2H_2$lines were assigned to fifty-three bands, most of them being newly reported. Using new or improved upper state parameters and vibrational transition moment squared and Herman-Wallis parameters, recommended line lists of acetylene were generated for each band by interpolation and limited extrapolation beyond the observations. We have included in **Fig. 7** a typical example of comparison of the measured acetylene spectrum to the line lists provided in the Acetylene Spectroscopic Databank [22]. The displayed region near 5840 cm^{-1} is located just below the range of our previous CRDS study above 5851 cm^{-1} [16] which were taken into account to derive the set of effective parameters used to generate the ASD. Significant deviations are noted in particular concerning line intensities (see **Fig. 3** for the line position comparison). Although providing a considerable higher number of lines (for instance 150 lines with intensity larger than 10^{-28} cm/molecule, to be compared to 26 in our list), the ASD relying on a global modeling approach of the $^{12}C_2H_2$ spectrum does not reach the accuracy of our empirical line list based on the usual band-by-band analysis. Nevertheless, as demonstrated in this work, the assignment of the present CRDS spectrum would not have been achieved without the high quality predictions of the ASD. In addition, the global approach has the advantage to be more complete, in particular for applications at high temperature. The large amount of new data obtained in this work will be valuable to further refine the EH and EDM effective parameters used to generate the ASD. Let us hope that future versions of the ASD will help to reduce the important number of lines remaining unassigned in our CRDS spectra.

Acknowledgements

The supports of the CNRS (France) and RFBR (N16-55-16017) in the frame of Laboratoire International Associé SAMIA are acknowledged. O.L thanks Université Grenoble Alpes for a two-months support at LIPhy Grenoble. This work was performed in the frame of the LabexOSUG@2020 (ANR10 LABX56) and of the ANR project e_PYTHEAS (ANR-16-CE31-0005).

References

1. Kellman ME and Tyng V. The dance of molecules: New dynamical perspectives on highly excited molecular vibrations," Acc. Chem. Res. 40, 243–250 (2007).
2. Herman M, Liévin J, Vander Auwera J, Campargue C. Global and accurate vibration hamiltonians from high-resolution molecular spectroscopy. Adv Chem Phys 1999;108:1–431. Wiley, New York.
3. Herman M, Campargue C, El Idrissi MI, Vander Auwera J. Vibrational spectroscopic database on acetylene, $\tilde{X}^1\Sigma_g^+$ ($^{12}C_2H_2$, $^{12}C_2D_2$ and $^{13}C_2H_2$) J Phys Chem Ref Data 2003;32:921–1361.
4. Fayt A, Robert S, Di Lonardo G, Fusina L, Tamassia F, Herman M. Vibration-rotation energy pattern in acetylene: $^{12}CH^{12}CH$ up to 6750 cm^{-1} J Chem Phys 2007;126:114303/1–8..
5. Campargue A; Temsamani MA; Herman M. The absorption spectrum of C_2H_2 between 12800 and 18000 cm^{-1}: I. Vibrational assignments. Molecular Physics 1997;90:793–805.
6. Yang SF; Biennier L; Campargue A; et al. The absorption spectrum of C_2H_2 between 12800 and 18000 cm^{-1}: II. Rotational analysis Molecular Physics 1997;90:807–16.
7. Gordon IE, Rothman LS, Hill C, Kochanov RV, Tan Y, Bernath PF, et al. The HITRAN2016 molecular spectroscopic database. J Quant Spectrosc Radiat Transfer 2017;203:3-69. https://doi.org/10.1016/j.jqsrt.2017.06.038
8. Zhan X, Vaittinen O, Halonen L. High-Resolution Photoacoustic Study of Acetylene Between 11 500 and 11 900 cm^{-1} Using a Titanium:Sapphire Ring Laser J. Molec Spectrosc 1993;160,172-180.
9. Keppler KA, Mellau G, Klee S, Winnewisser BP, Winnewisser M, Pliva J, et al. Precision measurements of acetylene spectra at 1.4–1.7 μm recorded with 352.5-m pathlength. J Mol Spectrosc 1996;175:411-20.
10. Robert S, Herman M, Fayt A, Campargue A, Kassi S, Liu A, et al. Acetylene, $^{12}C_2H_2$: new CRDS data and global vibration-rotation analysis up to 8600 cm^{-1}. Mol Phys 2008;106:2581–605.
11. Lyulin OM, Campargue A. An empirical spectroscopic database for acetylene in the regions of 5850-6341 cm^{-1} and 7000-9415 cm^{-1}. J Quant Spectrosc Radiat Transf 2017;203:461–471. 10.1016/j.jqsrt.2017.01.036
12. Lyulin OM, Vander Auwera J, Campargue A. The Fourier transform absorption spectrum of acetylene between 7000 and 7500 cm^{-1}. J Quant Spectrosc Radiat Transf 2015;160:85–93.
13. Lyulin OM, Vander Auwera J, Campargue A, The Fourier transform absorption spectrum of acetylene between 8280 and 8700 cm^{-1}. J Quant Spectrosc Radiat Transf 2016;177:234–240 http://dx.doi.org/10.1016/j.jqsrt.2015.11.026
14. Béguier S, Lyulin OM, Hu SM, Campargue A. Line intensity measurements for acetylene between 8980 and 9420 cm^{-1} J Quant Spectrosc Radiat Transf 2017;189:417-420. 10.1016/j.jqsrt.2016.12.020
15. Lyulin OM, Campargue A, Mondelain D, Kassi S. The absorption spectrum of acetylene by CRDS between 7244 and 7918 cm^{-1} J Quant Spectrosc Radiat Transf 2013;130:327–43.
16. Lyulin OM, Mondelain D, Béguier S, Kassi S, Vander Auwera J, Campargue A. High sensitivity absorption spectroscopy of acetylene by CRDS between 5851 and 6341 cm^{-1}. Mol Phys 2014;112:2433–44.
17. Kassi S, Lyulin OM, Béguier S, Campargue A. New assignments and a rare peculiarity in the high sensitivity CRDS spectrum of acetylene near 8000 cm^{-1}. J Mol Spectrosc 2016;326:106-114.
18. Jacquinet-Husson N, Armante R, Crépeau N, Chédin A, Scott NA, Boutammine C, et al. The 2015 edition of the GEISA spectroscopic database. J Mol Spectrosc 2016;327:31–72. doi:10.1016/j.jms.2016.06.007
19. Lyulin OM, Béguier S, Hu SM, Campargue A, The absorption spectrum of acetylene near 1 μm (9280–10740 cm^{-1}) (I): Line positions. J Quant SpectroscRadiatTransf 2018;208:179-187 DOI: 10.1016/j.jqsrt.2018.01.007
20. Lyulin OM, Campargue A. The absorption spectrum of acetylene near 1 μm (9280–10740 cm^{-1}) (II): Line intensities. J Quant Spectrosc Radiat Transf 2018;215:51-58. DOI: 10.1016/j.jqsrt.2018.04.025

21. Lyulin OM, Perevalov VI. Global modelling of vibration-rotation spectra of acetylene molecule. J Quant Spectrosc Radiat Transf 2016;177:59–74.
22. Lyulin OM, Perevalov VI. ASD-1000: High-resolution, high-temperature acetylene spectroscopic databank. J Quant Spectrosc Radiat Transf 2017;201:94–103.
23. Kassi S, Campargue A. Cavity ring down spectroscopy with 5×10^{-13} cm^{-1} sensitivity. J Chem Phys 2012;137:234201. doi: 10.1063/1.4769974
24. Mikhailenko SN, Mondelain D, Karlovets EV, Kassi S, Campargue A. Cavity Ring Down Spectroscopy of ^{17}O enriched water vapor near 1.73 µm. J Quant Spectrosc Radiat Transf 2019; 222–223:229–235.10.1016/j.jqsrt.2018.10.027
25. Bertin T, Mondelain D, Karlovets EV, Kassi S, Perevalov VI, Camargue A. High sensitivity cavity ring down spectroscopy of N_2O near 1.74 µm. J Quant Spectrosc Radiat Transf 2019 in press10.1016/j.jqsrt.2019.02.011
26. Čermák P, Karlovets EV, Mondelain D, Kassi S, Perevalov VI, Campargue A. High sensitivity CRDS of CO_2 in 1.74 µm transparency window. A validation test for the spectroscopic databases. J Quant Spectrosc Radiat Transf 2018;207:95–103.
27. Karlovets EV, Čermák P, Mondelain D, Kassi S, Campargue A, Tashkun SA, Perevalov VI. Analysis and theoretical modelling of the ^{18}O enriched carbon dioxide spectrum by CRDS near 1.74 µm. J Quant Spectrosc Radiat Transf 2018;217:73–85.
28. Lyulin OM, Jacquemart D, Lacome N, Perevalov VI, Mandin JY. Line parameters of acetylene in the 1.9 and 1.7 µm spectral regions J Quant Spectrosc Radiat Transfer 2008;109:1856-74.
29. Amyay B, Herman M, Fayt A, Campargue A, Kassi S. Acetylene, $^{12}C_2H_2$: refined analysis of CRDS spectra around 1.52 µm. J Mol Spectrosc 2011;267:80–91.
30. Di Lonardo G, Fusina L, Tamassia F, Fayt A, Robert S, Vander Auwera J, et al. The FT absorption spectrum of $^{13}CH^{12}CH$ (II): rotational analysis in the range 9500 to 10000 cm^{-1}. Mol Phys 2006;104:2617–2625.
31. Robert S. PhD thesis Université Libre de Bruxelles (2009).
32. Di Lonardo G, Baldan A, Bramati G, Fusina L. The infrared spectrum of $^{12}C^{13}CH_2$: the bending states up to v_4+v_5 =4. J Mol Spectrosc 2002;213:57–63.
33. Jacquemart D, Lacome N, Mandin JY, Dana V, Lyulin OM, Perevalov VI. Multispectrum fitting of line parameters for $^{12}C_2H_2$ in the 3.8-µm spectral region. J Quant Spectrosc Radiat Transf 2007;103:478-95.
34. Amyay B, Herman M, Fayt A, Fusina L, Predoi-Cross A. High resolution FTIR investigation of $^{12}C_2H_2$ in the FIR spectral range using synchrotron radiation. Chem. Phys. Lett. 2010;491:17-19.
35. Fischer J, Gamache RR, Goldman A, Rothman LS, Perrin A. Total internal partition sums for molecular species in the 2000 edition of the HITRAN database. J Quant Spectrosc Radiat Transfer 2003;82:401–12.
36. Perevalov VI, Lukashevskaya AA. Parameterization of the Effective Dipole Moment Matrix Elements in the Case of the Asymmetric Top Molecules. Application to NO_2 Molecule. Atmospheric and Oceanic Optics 2015;28:17–23.
37. Jacquemart D, Lacome N, Mandin J-Y, Dana V, Tran H, Gueye FK, Lyulin OM, Perevalov VI, Régalia-Jarlot L. The IR spectrum of $^{12}C_2H_2$: Line intensity measurements in the 1.4 µm region and update of the databases. J Quant Spectrosc Radiat Transf 2009;110:717-732. http://dx.doi.org/10.1016/j.jqsrt.2008.10.002

Table 1. Spectroscopic parameters (in cm^{-1}) of the rovibrational bands of $^{12}C_2H_2$ assigned in the*CW*-CRDSspectra of acetylene between 5693 and 6341 cm^{-1}. The bands are listed according to the increasing values of the upper state energy levels.

$^{12}C_2H_2$												
Lower levels												
$v_1v_2v_3v_4v_5l_4l_5\varepsilon$ [a]	G_c	$B_{e/f}$	$D_{e/f}\times10^6$	$H_{e/f}\times10^{10}$	n_{fit}/N_{tot} [b]	Bands [c]	*Band type*	ΔG_c [d]	*observed lines* [e]	*rms* [f]		Notes [g]
0000000	0.0	1.1766462	1.6270	0.016								
0001010e	611.693759	1.17532307	1.6405	0.0177								
0001010f	611.693755	1.18055377	1.67973	0.0187								
0000101e	729.15410	1.1764413	1.6326	0.017								
0000101f	729.15410	1.1811398	1.6714	0.018								
0002020f	1228.7997	1.179109	1.692									
0002020e	1228.8011	1.17908	19.0	245								
0002000	1230.3894	1.17937	-15.8	-246								
000111-1e	1328.0722	1.180508	3.595	2.76								
000111-1f	1340.5507	1.1800836	1.715									
0001111f	1342.8023	1.179838	1.647									
0001111e	1342.8034	1.179804	-0.226	-2.78								
0000200	1449.1107	1.181234	4.415	6.52								
0000202f	1458.2936	1.180757	1.669									
0000202e	1458.2944	1.180714	-1.052	-6.43								
0003030e	1851.3699	1.180358	10.15									
0003030f	1851.3749	1.18006	6.33	39								
0003010f	1854.5970	1.18583	-3.8	-61								
0003010e	1854.5978	1.17533	-6.2									
0002121f	1961.9321	1.180731	-1.03	-5.15								
0002121e	1961.9332	1.18069	-1.31	-10								
0000301f	2169.1559	1.188211	2.782	-1.89								
0000301e	2169.1575	1.178631	2.55	1.65								
0001212e	2074.1790(4)	1.181561(3)	1.056(4)		48/48	$(\nu_4+2\nu_5)^3$- $(2\nu_4+\nu_5)^3$	$\Phi_g-\Phi_u$	731.372(1)	P21/Q11/R27	0.6		Amy10
0001212f	2074.1807(5)	1.181533(7)	0.95(2)	1.7(2)	42/42	$(\nu_4+2\nu_5)^3$- $(2\nu_4+\nu_5)^3$	$\Phi_g-\Phi_u$	731.3803(8)	P17/Q10/R29	0.4		Amy10
1000000e	3372.8472(5)	1.169804(5)	1.62(1)		55/55	ν_1 - ν_5^1	$\Sigma_g^+-\Pi_u$	2643.6931(5)	P24/Q24/R22	0.07		Jacq07
Upper levels												
***P*=9**												
N 00140 2 0e	5719.758(4)	1.1769(1)	40(2)	733(45)	10/14	$\nu_3+4\nu_4^2$	$\Pi_u-\Sigma_g^+$	5719.758(4)	P11/R17	3.0	P	
00140 0 0e	5721.792(1)	1.17819(6)	-46.1(7)	-848(18)	17/33	$\nu_3+4\nu_4^0$	$\Sigma_u^+-\Sigma_g^+$	5721.792(1)	P12/R25	1.6	P	
02021 2-1f	5816.8621(5)	1.172502(3)	2.723(4)		29/29	$2\nu_2+(2\nu_4+\nu_5)^1\Pi$	$\Pi_u-\Sigma_g^+$	5816.8621(5)	Q29	0.5		HITRAN, Kep96
02021 2-1e	5816.8629(4)	1.165053(2)	2.576(3)	1.10(1)	66/71	$2\nu_2+(2\nu_4+\nu_5)^1\Pi$	$\Pi_u-\Sigma_g^+$	5816.8629(4)	P41/R43	0.9		HITRAN, Kep96
N 02021 0 1e	5840.5093(4)	1.170042(3)	2.988(2)		28/38	$2\nu_2+(2\nu_4+\nu_5)^1\Pi$	$\Pi_u-\Sigma_g^+$	5840.5093(4)	P33/R35	1.2		
N 02021 0 1f	5840.5143(8)	1.166782(7)	2.50(1)		14/19	$2\nu_2+(2\nu_4+\nu_5)^1\Pi$	$\Pi_u-\Sigma_g^+$	5840.5143(8)	Q25	1.8		

	02021 2 1e	5842.634(2)	1.16820(1)	0.38(2)		14/18	$2\nu_2+(2\nu_4+\nu_5)^3$	$\Phi_u - \Sigma_g^+$	5842.634(2)	P20/R25	1.5	**P**	
	02021 2 1f	5842.658(1)	1.16802(2)	0.30(5)		11/15	$2\nu_2+(2\nu_4+\nu_5)^3$	$\Phi_u - \Sigma_g^+$	5842.658(1)	Q25	0.8		
	01110 1 0e	5850.6471(6)	1.163361(7)	1.73(2)	8.0(1)	47/58	$\nu_2+\nu_3+\nu_4^1$	$\Pi_u - \Sigma_g^+$	5850.6471(6)	P34/R26	1.6		HITRAN, Kep96
	01110 1 0f	5850.6496(7)	1.169250(6)	1.25(1)	1.19(5)	38/38	$\nu_2+\nu_3+\nu_4^1$	$\Pi_u - \Sigma_g^+$	5850.6496(7)	Q38	0.9		HITRAN, Kep96
	10031 1-1e	5865.5601(6)	1.17874(1)	19.57(9)	132(1)	38/52	$\nu_1+(3\nu_4+\nu_5)^{0+}$	$\Sigma_u^+ - \Sigma_g^+$	5865.5601(6)	P31/R31	1.2	**P**	Lyu14, Amy11
	01033 1-1e	5893.2617(9)	1.18008(3)	22.1(2)	199(4)	18/28	$\nu_2+(3\nu_4+3\nu_5)^{0+}$II	$\Sigma_u^+ - \Sigma_g^+$	5893.2617(9)	P21/R19	1.6	**P**	Lyu14
	01033 3-3e	5921.9203(7)	1.17960(1)	3.25(8)	15(1)	34/35	$\nu_2+(3\nu_4+3\nu_5)^{0+}$I	$\Sigma_u^+ - \Sigma_g^+$	5921.9203(7)	P21/R20	1.0		
N	00122 0 0e	5943.5447(6)	1.178804(5)	1.984(6)		32/35	$\nu_3+(2\nu_4+2\nu_5)^0$I	$\Sigma_u^+ - \Sigma_g^+$	5943.5447(6)	P23/R34	1.0		
N	10013 1 1f	6090.361(2)	1.17868(1)	2.79(2)		9/9	$\nu_1+(\nu_4+3\nu_5)^2$II	$\Delta_u - \Sigma_g^+$	6090.361(2)	Q25	1.0		
N	10013 1 1e	6090.375(2)	1.17847(2)	-5.81(8)	-33.2(7)	17/20	$\nu_1+(\nu_4+3\nu_5)^2$II	$\Delta_u - \Sigma_g^+$	6090.375(2)	P26/R24	**1.7**	**P**	
	***P*=10**												
N	02031 3-1f	6409.5157(3)	1.169844(2)	2.427(2)		58/62	$2\nu_2+(3\nu_4+\nu_5)^2$II-ν_4^1	$\Pi_u - \Pi_g$	5797.8219(3)	P27/Q33/R27	1.3		
N	02031 3-1e	6409.5169(7)	1.16984(1)	13.61(8)	79(1)	43/57	$2\nu_2+(3\nu_4+\nu_5)^2$II-ν_4^1	$\Pi_u - \Pi_g$	5797.8231(7)	P31/Q20/R23	1.5	**P**	
	02031 1-1e	6413.8975(5)	1.17005(1)	-8.92(9)	-81(1)	45/47	$2\nu_2+(3\nu_4+\nu_5)^{0+}$-$\nu_4^1$	$\Sigma_u^+ - \Pi_g$	5802.2037(5)	P21/Q20/R19	1.1		
N	02031 3 1e	6443.845(6)	1.1735(1)	27.4(8)	395(14)	6/7	$2\nu_2+(3\nu_4+\nu_5)^4$-ν_4^1	$\Gamma_u - \Pi_g$	5832.151(6)	Q11/R16	0.3		
N	02031 3 1f	6444.164(3)	1.16754(8)	-4.9(6)	-90(11)	15/19	$2\nu_2+(3\nu_4+\nu_5)^4$-ν_4^1	$\Gamma_u - \Pi_g$	5832.470(3)	P17/Q16/R15	1.6		
	01120 2 0f	6447.8094(6)	1.16777(2)	-1.7(1)		28/45	$\nu_2+\nu_3+2\nu_4^2$-ν_4^1	$\Delta_u - \Pi_g$	5836.1156(6)	P23/Q20/R19	1.2	**P**	Lyu14, Kep96
	01120 2 0e	6447.8097(8)	1.16785(4)	27.1(6)	542(21)	28/58	$\nu_2+\nu_3+2\nu_4^2$-ν_4^1	$\Delta_u - \Pi_g$	5836.1159(8)	P24/Q30/R25	1.0	**P**	Lyu14, Kep96
	01120 0 0e	6449.1056(9)	1.16788(4)	-23.0(3)	-370(9)	31/39	$\nu_2+\nu_3+2\nu_4^0$-ν_4^1	$\Sigma_u^+ - \Pi_g$	5837.4118(9)	P17/Q16/R14	1.4		
	00200 0 0e	6502.3368(5)	1.166130(4)	3.313(8)	3.46(4)	89/91	$2\nu_3$- ν_5^1	$\Sigma_g^+ - \Pi_u$	5773.1827(5)	P29/Q37/R32	1.5		HITRAN, Kep96
N	11020 2 0f	6510.2596(9)	1.16660(1)	1.81(2)		11/11	$\nu_1+\nu_2+2\nu_4^2$-ν_5^1	$\Delta_g - \Pi_u$	5781.1055(9)	Q22	1.2		
N	11020 2 0e	6510.2626(5)	1.166620(7)	5.60(2)	17.2(2)	63/76	$\nu_1+\nu_2+2\nu_4^2$-ν_5^1	$\Delta_g - \Pi_u$	5781.1085(5)	P32/Q31/R31	1.5		
	11020 0 0e	6513.9918(4)	1.166582(5)	-3.20(2)	-20.0(1)	71/83	$\nu_1+\nu_2+2\nu_4^0$-ν_5^1	$\Sigma_g^+ - \Pi_u$	5784.8377(4)	P32/Q29/R28	0.9	**P**	HITRAN, Kep96
N	02022 2-2f	6533.0231(4)	1.170879(4)	2.689(8)		32/45	$2\nu_2+(2\nu_4+2\nu_5)^0$II -ν_5^1	$\Sigma_g^- - \Pi_u$	5803.8690(4)	P20/Q25/R19	1.3		
N	02022 0 0e	6560.7067(5)	1.170214(6)	0.82(2)	-46.0(1)	53/64	$2\nu_2+(2\nu_4+2\nu_5)^0$I-ν_5^1	$\Sigma_g^+ - \Pi_u$	5831.5526(5)	P31/Q28/R29	1.4		
	01111 1-1e	6562.4106(5)	1.168795(7)	5.66(2)	56.9(1)	59/62	$\nu_2+\nu_3+(\nu_4+\nu_5)^{0+}$-$\nu_5^1$	$\Sigma_g^+ - \Pi_u$	5833.2565(5)	P33/Q20/R20	1.4		Lyu14
	01111 1-1f	6569.6089(4)	1.168320(2)	1.252(1)		66/75	$\nu_2+\nu_3+(\nu_4+\nu_5)^{0-}$-$\nu_5^1$	$\Sigma_g^- - \Pi_u$	5840.4548(4)	P24/Q40/R27	1.2		Lyu14
	01111 1 1e	6573.796(1)	1.16813(2)	-5.03(9)	-38(1)	39/47	$\nu_2+\nu_3+(\nu_4+\nu_5)^2$-$\nu_5^1$	$\Delta_g - \Pi_u$	5844.642(1)	P18/Q29/R22	1.6	**P**	Lyu14
	01111 1 1f	6573.7996(9)	1.16803(2)	-3.27(9)	-28(1)	44/46	$\nu_2+\nu_3+(\nu_4+\nu_5)^2$-$\nu_5^1$	$\Delta_g - \Pi_u$	5844.6455(9)	P22/Q20/R21	1.0		Lyu14
N	02013-1 3f	6664.464(2)	1.17123(2)	2.79(6)		5/8	$2\nu_2+(\nu_4+3\nu_5)^2$II-ν_4^1	$\Delta_u - \Pi_g$	6052.770(2)	P15/Q18	0.4		
	02013-1 3e	6664.4677(9)	1.17117(2)	-3.65(4)		9/11	$2\nu_2+(\nu_4+3\nu_5)^2$II-ν_4^1	$\Delta_u - \Pi_g$	6052.7739(9)	P17/Q19/R05	2.1		
	02013 1-1f	6681.1586(5)	1.171364(6)	4.09(1)		26/33	$2\nu_2+(\nu_4+3\nu_5)^{0-}$-$\nu_4^1$	$\Sigma_u^- - \Pi_g$	6069.4648(5)	P20/Q19/R21	1.5		Lyu14[h]
N	02013 1 1f	6686.986(1)	1.17111(2)	-0.53(6)		9/9	$2\nu_2+(\nu_4+3\nu_5)^2$I-ν_4^1	$\Delta_u - \Pi_g$	6075.292(1)	Q12/R16	1.4		
	02013 1 1e	6686.991(2)	1.17099(5)	2.7(3)		10/10	$2\nu_2+(\nu_4+3\nu_5)^2$I-ν_4^1	$\Delta_u - \Pi_g$	6075.297(2)	Q12/R08	1.0		
N	00114-1 2e	6752.638(4)	1.18676(7)	2.4(3)		9/9	$\nu_3+(\nu_4+4\nu_5)^1$I- ν_4^1	$\Pi_u - \Pi_g$	6140.944(4)	P13/R13	0.8		
N	00114-1 2f	6752.639(1)	1.17603(1)	1.45(2)		14/16	$\nu_3+(\nu_4+4\nu_5)^1$I- ν_4^1	$\Pi_u - \Pi_g$	6140.945(1)	P24/R23	1.2		
N	10014 1 0f	6779.0509(6)	1.189411(8)	5.15(2)		20/20	$\nu_1+(\nu_4+4\nu_5)^1$II-ν_5^1	$\Pi_g - \Pi_u$	6049.8968(6)	P21/R19	1.4		
N	10014 1 0e	6779.0549(7)	1.17382(1)	3.90(4)		20/20	$\nu_1+(\nu_4+4\nu_5)^1$II-ν_5^1	$\Pi_g - \Pi_u$	6049.9008(7)	P18/R13	1.0		
	***P*=11**												

	02041 2-1f	7015.944(1)	1.17812(1)			7/7	$2\nu_2+(4\nu_4+\nu_5)^1II-2\nu_4^0$	$\Pi_u - \Sigma_g^+$	5785.554(1)	Q13	2.0		
N	01130 3 0e	7046.7106(9)	1.16883(1)	5.03(5)		17/22	$\nu_2+\nu_3+3\nu_4^3-2\nu_4^2$	$\Phi_u - \Delta_g$	5817.9095(9)	P13/Q17/R16	1.8		
N	01130 3 0f	7046.7146(8)	1.168742(7)	4.78(1)		20/28	$\nu_2+\nu_3+3\nu_4^3-2\nu_4^2$	$\Phi_u - \Delta_g$	5817.9149(8)	P19/Q15/R24	1.4		
	00210 1 0e	7091.2783(4)	1.164033(5)	2.28(2)	1.3(1)	45/48	$2\nu_3+ \nu_4^1- (\nu_4+\nu_5)^0$	$\Pi_g - \Sigma_u$	5763.2061(4)	P21/Q32/R24	1.1		
						38/46	$2\nu_3+ \nu_4^1- (\nu_4+\nu_5)^2$	$\Pi_u - \Delta_u$	5748.4749(4)	P19/Q30/R30	1.4		
	00210 1 0f	7091.2791(4)	1.171309(6)	2.97(2)	2.7(2)	46/49	$2\nu_3+ \nu_4^1- (\nu_4+\nu_5)^0$	$\Pi_g - \Sigma_u$	5750.7284(4)	P22/Q30/R21	1.3		
						44/44	$2\nu_3+ \nu_4^1- (\nu_4+\nu_5)^2$	$\Pi_u - \Delta_u$	5748.4768(4)	P21/Q28/R26	1.1		
N	11030 3 0e	7106.8768(6)	1.169753(5)	2.268(7)		13/13	$\nu_1+\nu_2+3\nu_4^3-(\nu_4+\nu_5)^2$	$\Phi_g - \Delta_u$	5764.0734(6)	P06/Q28/R20	1.8		
						3/3	$\nu_1+\nu_2+3\nu_4^3-(\nu_4+\nu_5)^0$	$\Phi_g - \Sigma_u$	5778.8046(6)	P09/Q26	1.8		
	02032 3-2f	7106.8782(4)	1.175387(3)	1.848(6)	-6.90(3)	32/43	$2\nu_2+(3\nu_4+2\nu_5)^1III-(\nu_4+\nu_5)^2$	$\Pi_g - \Delta_u$	5764.0759(4)	P27/Q30/R26	1.5		
						38/43	$2\nu_2+(3\nu_4+2\nu_5)^1III-(\nu_4+\nu_5)^0$	$\Pi_g - \Sigma_u$	5766.3275(4)	P25/Q30/R38	1.2		
	02032 3-2e	7106.9072(6)	1.163777(5)	2.999(9)		29/35	$2\nu_2+(3\nu_4+2\nu_5)^1III-(\nu_4+\nu_5)^2$	$\Pi_g - \Delta_u$	5764.1038(6)	P21/Q25/R17	1.4		
						14/21	$2\nu_2+(3\nu_4+2\nu_5)^1III-(\nu_4+\nu_5)^0$	$\Pi_g - \Sigma_u$	5778.8350(6)	P20/Q21	1.2		
N	11030 3 0f	7106.926(1)	1.16652(2)	2.02(7)		5/5	$\nu_1+\nu_2+3\nu_4^3-(\nu_4+\nu_5)^2$	$\Phi_g - \Delta_u$	5764.124(1)	P09/Q13/R15	1.8		
						4/4	$\nu_1+\nu_2+3\nu_4^3-(\nu_4+\nu_5)^0$	$\Phi_g - \Sigma_u^-$	5766.375(1)	P5-15	1.2		
	11021 2-1e	7205.9516(8)	1.16481(2)	2.66(6)		17/25	$\nu_1+\nu_2+(2\nu_4+\nu_5)^1II-2\nu_4^2$	$\Pi_u - \Delta_g$	5977.1505(8)	P17/Q14/R30	1.3	**P**	Lyu14
	11021 2-1f	7205.9518(5)	1.174934(2)	3.391(2)		25/35	$\nu_1+\nu_2+(2\nu_4+\nu_5)^1II-2\nu_4^2$	$\Pi_u - \Delta_g$	5977.1521(5)	P36/Q19/R34	1.1		Lyu14
	00201 0 1e	7218.1971(5)	1.166518	2.77(2)	3.6(2)	41/44	$2\nu_3+\nu_5^1- 2\nu_5^0$	$\Pi_u - \Sigma_g^+$	5769.0864(5)	P27/R28	1.1		
						51/51	$2\nu_3+\nu_5^1- 2\nu_5^2$	$\Pi_u - \Delta_g$	5759.9027(5)	P23/Q24/R18	1.2		
	00201 0 1f	7218.1999(5)	1.168850(4)	1.979(8)		19/22	$2\nu_3+\nu_5^1- 2\nu_5^0$	$\Pi_u - \Sigma_g^+$	5769.0892(5)	Q25	1.4		
						48/57	$2\nu_3+\nu_5^1- 2\nu_5^2$	$\Pi_u - \Delta_g$	5759.9063(5)	P25/Q24/R24	1.5		
	11021 2 1e	7228.0825(7)	1.167720(6)	2.66(1)		10/10	$\nu_1+\nu_2+(2\nu_4+\nu_5)^3-2\nu_5^0$	$\Phi_u - \Sigma_g^+$	5778.9718(7)	P25/R17	1.5		
						16/17	$\nu_1+\nu_2+(2\nu_4+\nu_5)^3-2\nu_5^2$	$\Phi_u - \Delta_g$	5769.7881(7)	P16/Q17/R12	1.5		
	11021 2 1f	7228.087(1)	1.168076(8)	2.34(1)		3/3	$\nu_1+\nu_2+(2\nu_4+\nu_5)^3-2\nu_5^0$	$\Phi_u - \Sigma_g^+$	5778.976(1)	Q27	1.7		
						11/15	$\nu_1+\nu_2+(2\nu_4+\nu_5)^3-2\nu_5^2$	$\Phi_u - \Delta_g$	5769.793(1)	P16/Q24/R24	1.7		
	01112 1 0e	7273.7685(9)	1.165424(8)	2.357(9)		17/19	$\nu_2+\nu_3+(\nu_4+2\nu_5)^1II-2\nu_5^2$	$\Pi_u - \Delta_g$	5815.4741(9)	P23/Q29/R08	1.3		
	01112 1 0f	7273.7698(7)	1.175806(5)	2.746(6)		26/29	$\nu_2+\nu_3+(\nu_4+2\nu_5)^1II-2\nu_5^2$	$\Pi_u - \Delta_g$	5815.4762(7)	P17/Q30/R16	1.6		
	11012 1 0f	7329.3443(9)	1.175580(8)	2.95(1)		18/19	$\nu_1+\nu_2+(\nu_4+2\nu_5)^1II- (\nu_4+\nu_5)^2$	$\Pi_g - \Delta_u$	5986.5420(9)	P07/Q16/R22	1.1		Lyu14
	11012 1 0e	7329.346(1)	1.16515(2)	2.45(4)		13/14	$\nu_1+\nu_2+(\nu_4+2\nu_5)^1II- (\nu_4+\nu_5)^2$	$\Pi_g - \Delta_u$	5986.543(1)	P08/Q19/R16	1.4		Lyu14
	***P*=12**												
	00220 2 0f	7685.477(2)	1.16875(3)			6/6	$2\nu_3+ 2\nu_4^2- (2\nu_4+\nu_5)^3$	$\Delta_g - \Phi_u$	5723.542(2)	P11/Q06	2.2		
	10120 0 0e	7732.787(1)	1.16841(6)	-30.2(8)	-802(30)	9/26	$\nu_1+\nu_3+2\nu_4^0- 3\nu_4^1$	$\Sigma_u^+ - \Pi_g$	5878.190(1)	P11/Q24	1.3	**P**	Lyu14
	020333-3e	7787.3234(8)	1.17206(2)	10.5(1)		14/14	$\nu_2+(3\nu_4+3\nu_5)^{0+}II-2\nu_5^0$	$\Sigma_u^+ - \Sigma_g^+$	6338.2127(8)	P15/R00	0.6		
	00202 0 0e	7922.109(1)	1.16983(1)	4.31(3)		21/23	$2\nu_3+2\nu_5^0- 3\nu_5^1$	$\Sigma_g^+ - \Pi_u$	5752.952(1)	P20/Q15/R20	1.4		
	20011 1 1f	8008.2364(8)	1.16664(1)	1.68(3)		14/14	$2\nu_1+(\nu_4+\nu_5)^2-3\nu_4^3$	$\Delta_u - \Phi_g$	6156.8615(8)	P21/Q17/R14	1.6		
	20011 1 1e	8008.2381(8)	1.16654(1)	-0.37(3)		12/12	$2\nu_1+(\nu_4+\nu_5)^2-3\nu_4^3$	$\Delta_u - \Phi_g$	6156.8682(8)	P18/Q20/R19	1.2		
	***P*=13**												
	10130 3 0e	8329.288(2)	1.16834(7)	37.2(5)		10/16	$\nu_1+\nu_3+3\nu_4^3- (\nu_4+2\nu_5)^3$	$\Phi_u - \Phi_g$	6255.113(2)	P10/Q11/R07	1.5	**P**	
N	10130 3 0f	8329.350(1)	1.16597(2)			7/9	$\nu_1+\nu_3+3\nu_4^3- (\nu_4+2\nu_5)^3$	$\Phi_u - \Phi_g$	6255.167(1)	P08/Q11/R06	2.2		

10130 1 0f	8330.033(2)	1.17611(5)	-2.0(4)	-33(8)	8/12	$\nu_1+\nu_3+3\nu_4^1-(\nu_4+2\nu_5)^3$	$\Pi_u-\Phi_g$	6255.850(2)	P18/R15	0.8	**P**
10130 1 0e	8330.050(2)	1.16371(7)	-39.2(7)	-790(17)	11/16	$\nu_1+\nu_3+3\nu_4^1-(\nu_4+2\nu_5)^3$	$\Pi_u-\Phi_g$	6255.875(2)	P17/R13	0.9	**P**
10121 2-1f	8419.5048(5)	1.174844(4)	3.435(5)		24/41	$\nu_1+\nu_3+(2\nu_4+\nu_5)^1\Pi-3\nu_5^1$	$\Pi_g-\Pi_u$	6250.3489(5)	P20/Q30/R19	1.1	**P**
10121 2-1e	8419.5068(5)	1.164895(6)	2.78(1)		19/26	$\nu_1+\nu_3+(2\nu_4+\nu_5)^1\Pi-3\nu_5^1$	$\Pi_g-\Pi_u$	6250.3493(5)	P16/ R27	1.3	
***P*=15**											
00300 0 0e	9639.8678(9)	1.15838(1)	1.79(2)		23/33	$3\nu_3-\nu_1$	$\Sigma_u^+-\Sigma_g^+$	6267.0206(9)	P25/R24	1.6	
$^{13}C^{12}CH_2$											
Lower levels											
00000 0 0	0.0	1.1484335	1.5256								
00010 1 0e	608.3535	1.147100	1.592								
00010 1 0f	608.3535	1.152127	1.640								
00001 0 1f	728.2282	1.152682	1.586								
00001 0 1e	728.2293	1.148195	1.544								
Upper levels											
00140 0 0	5713.179(3)	1.1481(1)	9.1(6)		11/11	$\nu_3+4\nu_4^0$	$\Sigma-\Sigma$	5713.179(3)	P08/R10	1.2	
02021 2-1e	5747.316(1)	1.13712(2)	2.46(3)		15/15	$2\nu_2+(2\nu_4+\nu_5)^1\Pi$	$\Pi-\Sigma$	5747.316(1)	P21/R22	1.8	
01110 1 0f	5807.5720(9)	1.140664(5)	1.538(5)		29/29	$\nu_2+\nu_3+\nu_4^1$	$\Pi-\Sigma$	5807.5720(9)	Q33	0.7	
01110 1 0e	5807.5721(8)	1.135477(6)	1.511(8)		40/40	$\nu_2+\nu_3+\nu_4^1$	$\Pi-\Sigma$	5807.5721(8)	P29/R27	1.0	
01120 2 0f	6400.041(3)	1.13910(2)	1.53(5)		15/15	$\nu_2+\nu_3+2\nu_4^2-\nu_4^1$	$\Delta-\Pi$	5791.688(3)	P22/Q20/R09	3.1	
01120 2 0e	6400.141(7)	1.13725(7)	6.2(2)		12/16	$\nu_2+\nu_3+2\nu_4^2-\nu_4^1$	$\Delta-\Pi$	5791.788(7)	P20/Q13/R16	3.3	
01120 0 0	6401.819(2)	1.14002(4)	-8.7(2)	-88(3)	16/16	$\nu_2+\nu_3+2\nu_4^0-\nu_4^1$	$\Sigma^-\Pi$	5793.466(2)	P11/Q22/R04	5.5	**P**
002000 0	6492.8545(6)	1.137375(6)	1.418(9)		60/63	$2\nu_3-\nu_5^1$	$\Sigma^-\Pi$	5764.6252(6)	P26/Q27/R26	2.2	
01111 1-1e	6518.2049(9)	1.139926(9)	3.42(2)		29/29	$\nu_2+\nu_3+(\nu_4+\nu_5)^{0+}-\nu_5^1$	$\Sigma^-\Pi$	5789.9756(9)	P24/Q24/R16	2.7	
10100 0 0	6542.879(2)	1.13631(2)	1.57(5)		14/14	$\nu_1+\nu_3-\nu_5^1$	$\Sigma^-\Pi$	5814.650(2)	P21/Q19/R12	1.3	

Notes

The spectroscopic parameters are given in cm^{-1}. The confidence interval (1 SD) is given in parenthesis in the unit of the last quoted digit.

[a] Normal mode labeling: $v_{i=1-5}$ are the vibrational quantum numbers, $l_{4,5}$ are the vibrational angular momentum quantum numbers associated to the degenerate bending modes and $\varepsilon=e$ or f is the symmetry type relative to the Wang transformation. The labeling was obtained according to the maximum value of the modulo of the expansion coefficients of the vibrational eigenfunction in the normal mode basis (for low J values). In two cases, the vibrational labeling has been chosen to avoid duplication (see Text, Section 3). "N" marks upper states newly observed.

[b] N_{tot} is the total number of the observed transitions reaching a given vibrational state and n_{fit} is the number of positions included in the fit of the parameters.

[c] Observed band in Plíva's notation

[d] Band center. $\Delta G_c = G_c^{'} - G_c^{''}$

[e] Observed branches with the maximum value or, in some cases, with the range of the total angular momentum quantum number.

[f] Root mean square deviation in 10^{-3} cm^{-1} unit. "P" marks perturbed states.

[g] Amy10 [34] and Jacq07 [33] correspond to the source of line positions used to fit the listed lower state parameters, "HITRAN" indicates the six bands included in the HITRAN20116 database [7]; Lyu14 [16], Kep96 [9] and Amy11 [29] mark bands which were previously reported in these references.

[h] The assignment of the band $2\nu_2+(\nu_4+3\nu_5)^{0-}-\nu_4^1$ centered at 6069.4648 cm^{-1} has been changed compared to Ref. [16].

Table 2. Vibrational transition dipole moment squared and Herman-Wallis coefficients of the acetylene bands assigned in this work. When available, the values previously obtained and used to generate the spectroscopic database of Ref. [16] (Lyu17) are given for comparison.

Band[a]	ΔG_c[b]	N_{exp}[c]	*rms (%)* [d]	N_{tot}[e]	Transitions [f]	$\|R_0\|^2$ *in* D^2	$A_1^{PR}\times10^2$	$A_2^{PR}\times10^3$	$A_2^{Q}\times10^3$	Ins.*%*[g]
C_2H_2										
00140 2 0 – 00000 0 0	5719.76	8	5.7	27	P12/R17	3.7(2)E-12		0.3(2)		7
00140 0 0 – 00000 0 0	5721.79	23	5.3	39	P13/R25	1.47(3)E-09	0.32(8)	-0.49(5)		7
00220 2 0f – 00021 2 1	5723.54	6	6.6	15	P12/Q07	8.6(3)E-07				15
00210 1 0e – 00011 1 1	5748.47	28	4.7	74	P20/Q31/R31	6.77(7)E-07	-0.29(4)		0.14(3)	7
00210 1 0f – 00011 1 1	5748.48	25	6.3	75	P22/Q29/R27	7.7(1)E-07	-0.58(7)		0.43(4)	7
00210 1 0 – 00011 1-1f	5750.73	24	4.9	78	P23/Q33/R22	6.19(7)E-07	-0.36(6)			7
00202 0 0 – 00003 0 1	5752.95	10	20.8	58	P21/Q16/R21	3.4(2)E-06				50
00201 0 1e – 00002 0 2	5759.90	39	4.5	65	P24/Q25/R19	1.35(2)E-06	-0.51(4)	-0.29(3)	0.14(3)	7
00201 0 1f – 00002 0 2	5759.91	32	4.4	69	P25/Q25/R25	1.37(1)E-06	-0.33(4)		0.37(3)	7
00210 1 0 – 00011 1-1e	5763.21	26	4.8	77	P21/Q31/R25	4.97(8)E-07	-0.52(6)	0.65(6)	0.39(5)	7
02032 3-2 - 00011 1 1e	5764.09	19	5.0	68	P22/Q31/R18	4.44(6)E-07			0.52(4)	7
02032 3-2 - 00011 1 1f	5764.09	15	8.0	78	P28/Q26/R27	3.7(1)E-07			-0.40(8)	10
11030 3 0 - 00011 1 1	5764.1	10	42	34	P09/Q28/R20	0.7(1)E-07				50
02032 3-2 - 00011 1-1f	5766.32	15	5.3	87	P26/Q22/R39	3.22(6)E-07			0.6(1)	10
00201 0 1 – 00002 0 0	5769.08	34	5.1	83	P28/Q26/R29	1.47(2)E-06	-0.43(5)	0.64(4)	-0.52(4)	7
11021 2 1 - 00002 0 2	5769.79	22	43	70	P17/Q24/R25	1.9(2)E-07				50
11030 3 0 - 00011 1-1	5772	7	68	7	P15/Q26	0.5(2)E-09				50
00200 0 0 – 00001 0 1	5773.18	70	4.0	101	P30/Q38/R33	1.152(6)E-06	-0.47(2)			5
02032 3-2 - 00011 1-1e	5778.83	16	7.9	51	P21/Q31	6.6(2)E-07			-0.58(6)	10
11021 2 1 - 00002 0 0	5778.97	7	28	13	P25/Q27/R17	1.2(2)E-09				50
11020 2 0 - 00001 0 1e	5781.11	28	12	82	P32/Q23/R31	7.2(3)E-09	-4.2(4)	16.4(6)		20
11020 2 0 - 00001 0 1f	5781.11	11	44	25	Q31	7.2(3)E-09			9(1)	50
11020 0 0 - 00001 0 1	5784.84	69	4.2	92	P33/Q30/R29	1.161(8)E-06	-0.38(2)	-0.459(9)	-0.39(1)	5
02041 2-1f - 00020 0 0	5785.55	5	2.5	14	Q14	7.9(3)E-08			0.8(2)	10
02031 3-1e - 00010 1 0	5797.82	31	6.9	70	P31/Q21/R23	3.48(7)E-08	-0.54(7)	0.69(5)	-1.42(6)	10
02031 3-1f - 00010 1 0	5797.82	40	4.1	87	P28/Q34/R28	3.22(3)E-08	-0.23(3)	0.16(2)	0.32(3)	7
02031 1-1 - 00010 1 0	5802.20	24	5.8	63	P22/Q21/R20	2.84(6)E-08	-0.63(4)	-1.47(3)	1.31(8)	10
02022 2-2f - 00001 0 1	5803.87	15	6.7	67	P21/Q26/R20	1.84(4)E-08			0.5(1)	10
01112 1 0 – 00002 0 2	5815.47	24	41	123	P24/Q31/R17	1.6(2)E-07				50
02021 2-1 - 00000 0 0	5816.86	74	3.8	116	P42/Q30/R44	2.65(1)E-08	-0.24(2)			5
01130 3 0 – 00020 2 0	5817.91	24	9.3	97	P20/Q18/R25	1.23(3)E-07	-0.4(1)	0.5(1)		15
02022 0 0 - 00001 0 1	5831.55	31	5.4	87	P32/Q29/R29	5.39(5)E-08		3.08(8)	1.45(6)	7
02031 3 1 - 00010 1 0	5832.3	11	42	51	P18/Q17/R17	2.4(4)E-11				50
01111 1-1e – 00001 0 1	5833.26	41	5.4	76	P34/Q21/R21	2.03(3)E-07	-0.31(4)	-0.38(3)	-0.94(4)	10
01111 1-1e – 00001 0 1	*5833.25*	*11*	*4.06*	*23*	*R23*	*2.5(1)E-07*	*-1.1(1)*			*Lyu17*
01120 2 0e – 00010 1 0	5836.12	37	20	67	P24/Q25/R25	1.01(5)E-07	-0.4(2)	0.4(1)	-4.51(8)	50

01120 2 0f – 00010 1 0	5836.12	31	4.4	52	P23/Q20/R19	9.8(1)E-08	-0.41(4)	-0.48(4)	-0.56(4)	7
01120 2 0 – 00010 1 0	*5836.12*			*19*	*R19*					*Lyu17*
01120 0 0 – 00010 1 0	5837.41	20	8.7	49	P18/Q17/R14	8.6(3)E-08	-1.6(2)	-5.1(2)	1.5(2)	15
01111 1-1f – 00001 0 1	5840.45	30	5.6	94	P25/Q41/R28	5.7(1)E-08		0.26(3)	0.61(7)	10
01111 1-1f – 00001 0 1	*5840.45*	*10*	*5.45*	*29*	*R29*	*6.9(1)E-08*				*Lyu17*
02021 0 1 - 00000 0 0	5840.51	33	7.9	76	P33/Q26/R35	1.16(3)E-09	-0.65(8)	-1.42(5)	0.47(7)	15
02021 2 1 - 00000 0 0	5842.65	17	8.0	48	P21/Q25/R26	8.4(9)E-13		4.2(4)	4.6(5)	20
01111 1 1e – 00001 0 1	5844.64	25	8.0	65	P19/Q29/R23	5.3(1)E-08		-1.07(6)	0.31(6)	10
01111 1 1f – 00001 0 1	5844.65	33	4.5	63	P23/Q21/R22	5.43(7)E-08	-0.55(4)	-0.42(3)	-0.47(4)	10
01111 1 1 – 00001 0 1	*5844.65*	*17*	*4.10*	*43*	*R23*	*6.1(1)E-08*	*-1.14(7)*			*Lyu17*
01110 1 0 – 00000 0 0	5850.65	86	3.1	100	P35/Q39/R26	1.103(6)E-07	-0.22(1)	-0.033(7)	-0.085(6)	5
10031 1-1 - 00000 0 0	5865.56	35	4.8	53	P31/R31	2.77(3)E-09	0.47(3)	-0.24(2)		5
10031 1-1 - 00000 0 0	*5865.56*	*18*	*4.53*	*27*	*P4/R22*	*2.90(3)E-09*				*Lyu17*
10120 0 0 - 00030 1 0	5878.19	11	3.1	34	P12/Q24	2.01(4)E-06	2.6(2)		0.73(5)	7
10120 0 0 - 00030 1 0	*5878.19*			*14*	*P08/Q24/R08*					*Lyu17*
01033 1-1 – 00000 0 0	5893.26	25	4.2	43	P22/R20	2.03(3)E-09	0.26(4)	-0.39(3)		7
01033 1-1 – 00000 0 0	*5893.26*	*24*	*3.6*	*35*	*P18/R16*	*2.12(2)E-09*		*-0.50(4)*		*Lyu17*
01033 3-3 – 00000 0 0	5921.92	25	4.9	44	P22/R21	7.09(7)E-10				7
00122 0 0 – 00000 0 0	5943.54	23	3.7	60	P24/R35	2.25(2)E-10	-0.11(3)			7
11021 2-1e - 00020 2 0	5977.15	14	9.4	51	P17/Q15/R30	4.3(2)E-08	0.9(2)			20
11021 2-1f - 00020 2 0	5977.15	19	12	68	P36/Q19/R34	4.1(1)E-08	-0.7(1)		-5.0(1)	20
11021 2-1 - 00020 2 0	*5977.15*			*49*	*P29/Q20/R34*					*Lyu17*
11012 1 0 - 00011 1 1	5986.54	17	5.1	88	P09/Q20/R23	8.6(4)E-11	-1.07(7)			7
11012 1 0 - 00011 1 1	*5986.54*			*21*	*P7/Q24/R22*					*Lyu17*
11002 0 2 - 00001 0 1	6039.37	12	4.3	67	Q26/R28	8.6(4)E-11		3.0(2)	3.9(2)	10
10014 1 0 - 00001 0 1	6049.90	24	4.2	73	P22/R20	4.10(4)E-10	-0.89(4)			7
02013-1 3 - 00010 1 0	6052.77	6	9.9	32	P17/Q19/R06	4.0(3)E-11		5(1)		50
02013 1 1 – 00010 1 0	6075.29	14	7.4	50	Q13/R17	8.1(3)E-11			0.7(2)	10
02013 1-1 - 00010 1 0	6069.46	19	9.5	52	P20/Q19/R21	1.20(4)E-10	-1.0(2)	0.8(1)		15
10013 1 1 - 00000 0 0	6090.37	14	5.4	68	P27/Q26/R25	4.1(2)E-14	-2.51(9)	1.10(7)	-4.30(5)	10
00114-1 2 – 00010 1 0	6140.94	12	8.8	75	P25/R24	3.5(1)E-11	-1.4(1)			10
20011 1 1 - 00030 3 0	6156.86	9	7.9	47	P21/Q20/R19	1.05(3)E-08				30
10121 2-1 - 00030 1 0	6250.35	23	9.6	96	P21/Q30/R28	1.10(4)E-07	0.9(1)	0.6(1)		15
10130 3 0 - 00012 1 2	6255.14	9	6.5	45	P11/Q12/R08	2.7(1)E-07	1.6(4)	-1.8(5)		20
10130 1 0 - 00012 1 2	6255.86	18	73	28	P18/R15	2.4(6)E-10				50
00300 0 0 – 10000 0 0	6267.02	15	9.3	51	P25/R25	9.3(2)E-05				15
020333-3 - 00002 0 0	6338.21	8	6.7	17	P16/R00	2.87(7)E-07				10
$^{13}C^{12}CH_2$										
00140 0 0 – 00000 0 0	5713.18	6	14	21	P09/R11	2.1(1)E-08				40
02021 2-1 – 00000 0 0	5747.32	10	13	45	P22/R23	5.9(3)E-08	-0.5(2)			20
00200 0 0 – 00001 0 1	5764.63	40	5.4	82	P27/Q28/R27	1.39(2)E-05	-0.41(5)	0.08(3)		10

01111 1-1 – 00001 0 1	5789.98	29	22	67	P25/Q25/R17	3.2(1)E-06				50
01120 2 0 – 00010 1 0	5791.73	14	9.9	94	P21/Q20/R16	8.4(3)E-07		2.3(2)		20
01120 0 0 – 00010 1 0	5793.47	7	5.7	40	P12/Q23/R05	7.2(4)E-07			1.5(2)	20
01110 1 0 – 00000 0 0	5807.57	43	4.9	92	P30/Q34/R28	8.85(7)E-07	-0.37(4)			7
10100 0 0 – 00001 0 1	5814.65	14	55	55	P22/Q20/R13	1.3(2)1E-06				50

Notes

[a] Band vibrational labeling, ($V_1V_2V_3V_4V_5l_4l_5$)

[b] Band center in cm^{-1}

[c] $N_{exp}$is the total number of measured line intensities included in the fit of the Herman-Wallis coefficients.

[d] Root mean square deviation of the intensity fit in %

[e] N_{tot} is the total number of lines included in our recommended list (SupMat II) including those with calculated and purely experimental line parameters.

[f] Maximum *J* value included in the database for the *P*, *Q* and *R* branches of each band.

[g] Estimated uncertainty of the line intensities values given in the recommended line list (SupMat II).

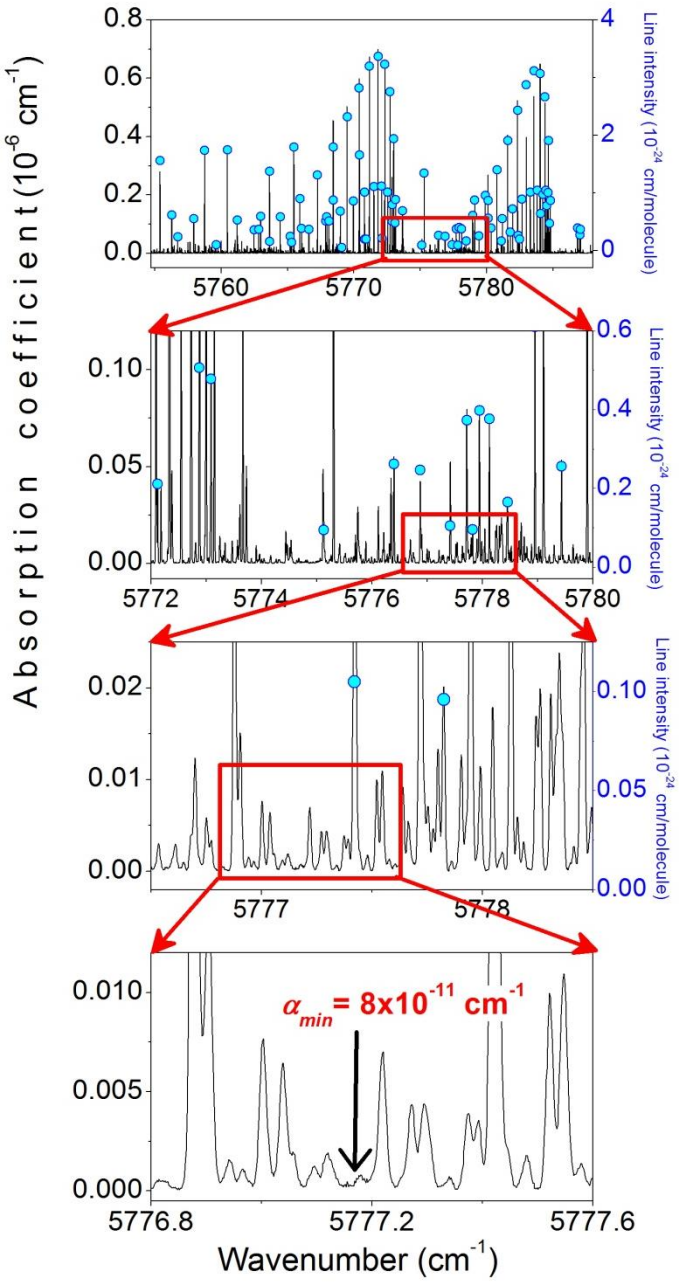
Absorption coefficient (10^{-6} cm^{-1})
Line intensity (10^{-24} cm/molecule)
α_{min} = 8x10^{-11} cm^{-1}
Wavenumber (cm^{-1})

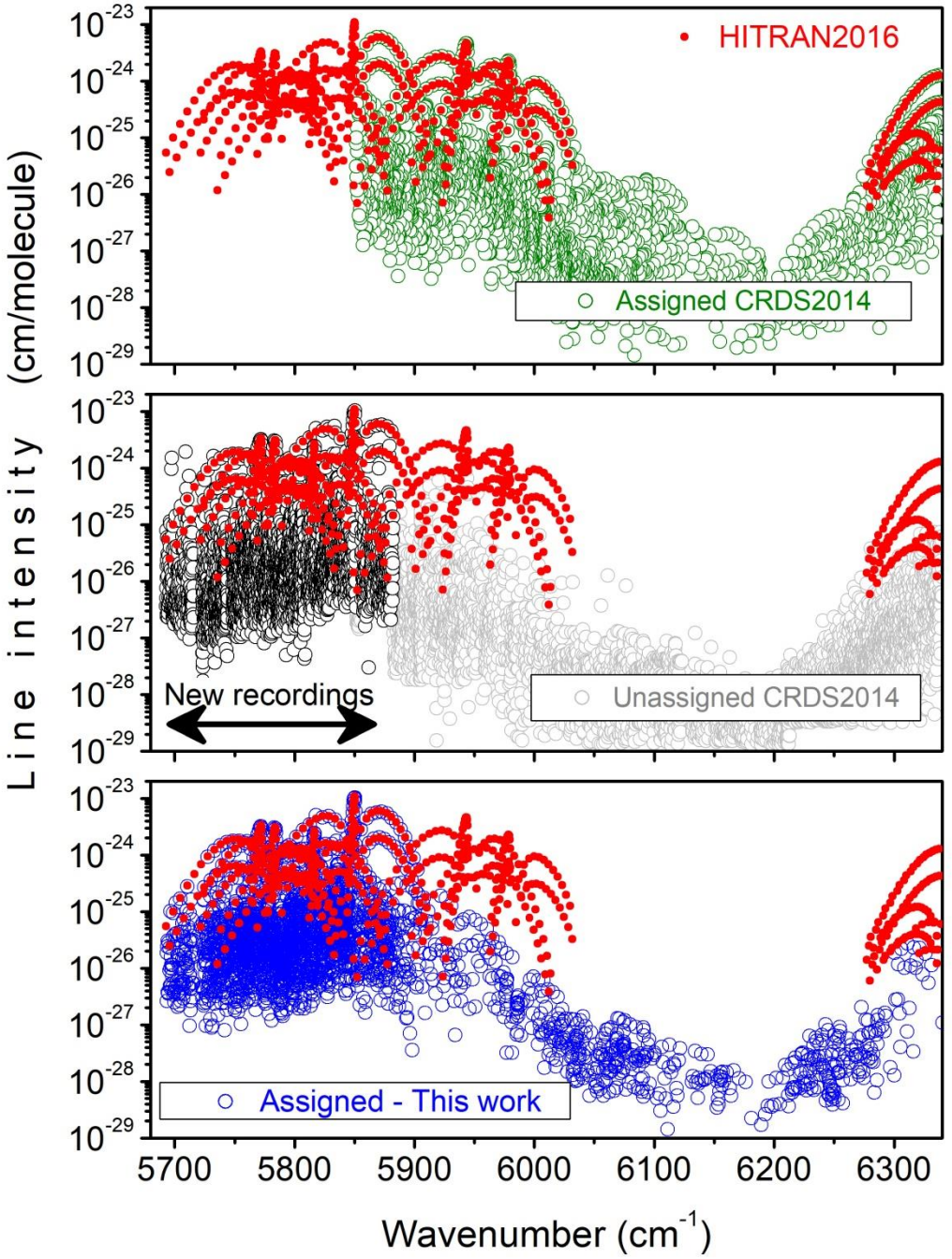
Line intensity (cm/molecule)
HITRAN2016
Assigned CRDS2014
New recordings
Unassigned CRDS2014
Assigned - This work
Wavenumber (cm^{-1})